Inorg. Chem. **2006**, *45*, 3905–3919

Coordination Chemistry of Tetradentate N-Donor Ligands Containing Two Pyrazolyl–Pyridine Units Separated by a 1,8-Naphthyl Spacer: Dodecanuclear and Tetranuclear Coordination Cages and Cyclic Helicates

Stephen P. Argent,[†] Harry Adams,[†] Thomas Riis-Johannessen,[‡] John C. Jeffery,[‡] Lindsay P. Harding,[§] Olimpia Mamula,[||] and Michael D. Ward*,[†]

Department of Chemistry, University of Sheffield, Sheffield S3 7HF, U.K., School of Chemistry, University of Bristol, Cantock's Close, Bristol BS8 1TS, U.K., Department of Chemical and Biological Sciences, University of Huddersfield, Huddersfield HD1 3DH, U.K., and Institute of Chemical Sciences and Engineering, Swiss Federal Institute of Technology, CH-1015 Lausanne, Switzerland

Received January 27, 2006

The tetradentate ligand L^{naph} contains two N-donor bidentate pyrazolyl–pyridine units connected to a 1,8-naphthyl core via methylene spacers; L^{*45} and L^{*56} are chiral ligands with a structure similar to that of L^{naph} but bearing pinene groups fused to either C^4 and C^5 or C^5 and C^6 of the terminal pyridyl rings. The complexes $[Cu(L^{naph})](OTf)$ and $[Ag(L^{naph})](BF_4)$ have unremarkable mononuclear structures, with Cu^I being four-coordinate and Ag^I being two-coordinate with two additional weak interactions (i.e., "2 + 2" coordinate). In contrast, $[Cu_4(L^{naph})_4][BF_4]_4$ is a cyclic tetranuclear helicate with a tetrafluoroborate anion in the central cavity, formed by an anion-templating effect; electrospray mass spectrometry (ESMS) spectra show the presence of other cyclic oligomers in solution. The chiral ligands show comparable behavior, with $[Cu(L^{*45})](BF_4)$ and $[Ag(L^{*45})](ClO_4)$ having similar mononuclear crystal structures and with the ligands being tetradentate chelates. In contrast, $[Ag_4(L^{*56})_4](BF_4)_4$ is a cyclic tetranuclear helicate in which both diastereomers of the complex are present in the crystal; the two diastereomers have similar gross geometries but are significantly different in detail. Despite their different crystal structures, $[Ag(L^{*45})](ClO_4)$ and $[Ag_4(L^{*56})_4](BF_4)_4$ behave similarly in solution according to ESMS studies, with a range of cyclic oligomers (up to Ag_9L_9) forming. With transition-metal dications Co^{II}, Cu^{II}, and Cd^{II}, L^{naph} generates a series of unusual dodecanuclear coordination cages $[M_{12}(L^{naph})_{18}]X_{24}$ ($X^- = ClO_4^-$ or BF_4^-) in which the 12 metal ions occupy the vertices of a truncated tetrahedron and a bridging ligand spans each of the 18 edges. The central cavity of each cage can accommodate four counterions, and each cage molecule is chiral, with all 12 metal trischelates being homochiral; the crystals are racemic. Extensive aromatic stacking between ligands around the periphery of the cages appears to be a significant factor in their assembly. The chiral analogue L^{*45} forms the simpler tetranuclear, tetrahedral coordination cage $[Zn_4(L^{*45})_6](ClO_4)_8$, with one anion in the central cavity; the steric bulk of the pinene chiral auxiliaries prevents the formation of a dodecanuclear cage, although trace amounts of $[Zn_{12}(L^{*45})_{18}](ClO_4)_{24}$ can be detected in solution by ESMS. Formation of $[Zn_4(L^{*45})_6](ClO_4)_8$ is diastereoselective, with the chirality of the pinene groups controlling the chirality of the tetranuclear cage.

Introduction

Coordination rings and cages have achieved recent prominence because of a combination of (i) their aesthetically appealing structures, (ii) the insight they give into understanding how control of self-assembly processes can afford elaborate structures from simple constituents, and (iii) the host–guest chemistry that results from incorporation of small molecules or anions in their central cavities.[1−8] Two-dimensional rings are exemplified by the cyclic helicates, which have been reported by Lehn, Constable, von Zelewsky, and others, in which, in some cases, a cyclic oligomer M_xL_y of a particular size forms because it is templated by a

* To whom correspondence should be addressed. E-mail: m.d.ward@sheffield.ac.uk.
[†] University of Sheffield.
[‡] University of Bristol.
[§] University of Huddersfield.
[||] Swiss Federal Institute of Technology.

10.1021/ic060157d CCC: $33.50
Published on Web 04/11/2006

counterion of the correct size for the central cavity.[8] Three-dimensional polyhedral cages have grown in complexity over the last 2 decades[1−7] from the tetrahedral cages first described by Saalfrank[4d,e] to enormously elaborate structures based on, e.g., octahedral,[3a] cubic,[6e] dodecahedral,[5f] truncated-tetrahedral,[5b,6c] and cuboctahedral[5g,6g] assemblies of metal ions. As with the cyclic helicates, some of these result from a templating effect of a counterion or other guest molecules of the correct size and shape to match the central cavity; in other cases, the formation of the cage is controlled by a judicious combination of the metal ion and bridging ligand, with the cage displaying host−guest behavior with a range of different guests.[1−7]

Chart 1

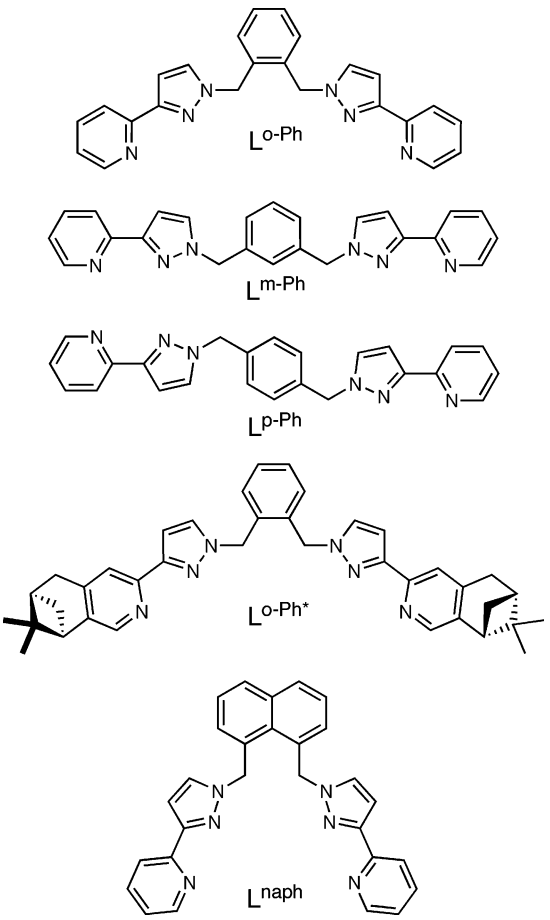

We have been especially interested in cage complexes formed by the reaction of bridging ligands containing bidentate chelating pyrazolyl−pyridine termini with labile six-coordinate metal ions.[6] The combination of tetradentate ligands with metal ions requiring six donor atoms results, necessarily, in the formation of complexes whose stoichiometry is M_2L_3 or some higher multiple thereof. Using ligands of the type shown in Chart 1, we have found that simple variation of the aromatic spacer used to connect the two coordinating arms results in quite dramatic and unpredictable variations in the structures of their complexes with divalent first-row transition-metal cations. Thus, L^{o-Ph} affords with Zn^{II} and Co^{II} tetrahedral cages $[M_4(L^{o-Ph})_6]^{8+}$,[6b] whose formation is templated by the presence of an anion (tetrafluoroborate or perchlorate) that is a good fit for the central cavity of the cage.[6d] Simply changing the central aromatic spacer from *o*- to *m*-phenylene results instead in cubic cage

(1) (a) Swiegers, G. F.; Malefetse, T. J. *Coord. Chem. Rev.* **2002**, *225*, 91. (b) Holliday, B. J.; Mirkin, C. A. *Angew. Chem., Int. Ed.* **2001**, *40*, 2022. (c) Cotton, F. A.; Lin, C.; Murillo, C. A. *Acc. Chem. Res.* **2001**, *34*, 759. (d) MacGillivray, L. R.; Atwood, J. L. *Angew. Chem., Int. Ed.* **1999**, *38*, 1019. (e) Amijs, C. H. M.; van Klink, G. P. M.; van Koten, G. *Dalton Trans.* **2006**, 308. (f) Alvarez, S. *Dalton Trans.* **2006**, 2209.

(2) (a) Fiedler, D.; Leung, D. H.; Bergman, R. G.; Raymond, K. N. *Acc. Chem. Res.* **2005**, *38*, 349. (b) Bruckner, C.; Powers, R. E.; Raymond, K. N. *Angew. Chem., Int. Ed.* **1998**, *37*, 1839. (c) Caulder, D. L.; Powers, R. E.; Parac, T. N.; Raymond, K. N. *Angew. Chem., Int. Ed.* **1998**, *37*, 1840. (d) Saalfrank, R. W.; Glaser, H.; Demleitner, B.; Hampel, F.; Chowdhry, M. M.; Schunemann, V.; Trautwein, A. X.; Vaughan, G. B. M.; Yeh, R.; Davis, A. V.; Raymond, K. N. *Chem.—Eur. J.* **2002**, *8*, 493. (e) Fiedler, D.; Bergman, R. G.; Raymond, K. N. *Angew. Chem., Int. Ed.* **2004**, *43*, 6748. (f) Davis, A. V.; Raymond, K. N. *J. Am. Chem. Soc.* **2005**, *127*, 7912.

(3) (a) Fujita, M.; Tominaga, M.; Hori, A.; Therrien, B. *Acc. Chem. Res.* **2005**, *38*, 369. (b) Yoshizawa, M.; Fujita, M. *Pure Appl. Chem.* **2005**, *77*, 1107. (c) Fujita, M.; Umemoto, K.; Yoshizawa, M.; Fujita, N.; Kusukawa, T.; Biradha, K. *Chem. Commun.* **2001**, 509. (d) Umemoto, K.; Tsukui, H.; Kusukawa, T.; Biradha, K.; Fujita, M. *Angew. Chem., Int. Ed.* **2001**, *40*, 2620. (e) Yoshizawa, M.; Kumazawa, K.; Fujita, M. *J. Am. Chem. Soc.* **2005**, *127*, 13456.

(4) (a) Saalfrank, R. W.; Demleitner, B.; Glaser, H.; Maid, H.; Reihs, S.; Bauer, W.; Maluenga, M.; Hampel, F.; Teichert, M.; Krautscheid, H. *Eur. J. Inorg. Chem.* **2003**, 822. (b) Saalfrank, R. W.; Demleitner, B.; Glaser, H.; Maid, H.; Bathelt, D.; Hampel, F.; Bauer, W.; Teichert, M. *Chem.—Eur. J.* **2002**, *8*, 2679. (c) Johnson, D. W.; Xu, J. D.; Saalfrank, R. W.; Raymond, K. N. *Angew. Chem., Int. Ed.* **1999**, *38*, 2882. (d) Saalfrank, R. W.; Burak, R.; Breit, A.; Stalke, D.; Herbst-Irmer, R.; Daub, J.; Porsch, M.; Bill, E.; Muther, M.; Trautwein, A. X. *Angew. Chem., Int. Ed. Engl.* **1994**, *33*, 1621. (e) Saalfrank, R. W.; Stark, A.; Bremer, M.; Hummel, H. U. *Angew. Chem., Int. Ed. Engl.* **1990**, *29*, 311.

(5) (a) Seidel, S. R.; Stang, P. J. *Acc. Chem. Res.* **2002**, *35*, 972. (b) Schweiger, M.; Yamamoto, T.; Stang, P. J.; Blaser, D.; Boese, R. *J. Org. Chem.* **2005**, *70*, 4861. (c) Mukherjee, P. S.; Das, N.; Stang, P. J. *J. Org. Chem.* **2004**, *69*, 3526. (d) Kuehl, C. J.; Kryschenko, Y. K.; Radhakrishnan, U.; Seidel, S. R.; Huang, S. D.; Stang, P. J. *Proc. Natl. Acad. Sci. U.S.A.* **2002**, *99*, 4932. (e) Leininger, S.; Fan, J.; Schmitz, M.; Stang, P. J. *Proc. Natl. Acad. Sci. U.S.A.* **2000**, *97*, 1380. (f) Olenyuk, B.; Levin, M. D.; Whiteford, J. A.; Shield, J. E.; Stang, P. J. *J. Am. Chem. Soc.* **1999**, *121*, 10434. (g) Olenyuk, B.; Whiteford, J. A.; Fechtenktter, A.; Stang, P. J. *Nature* **1999**, *398*, 796.

(6) (a) Amoroso, A. J.; Jeffery, J. C.; Jones, P. L.; McCleverty, J. A.; Thornton, P.; Ward, M. D. *Angew. Chem., Int. Ed. Engl.* **1995**, *34*, 1443. (b) Fleming, J. S.; Mann, K. L. V.; Carraz, C.-A.; Psillakis, E.; Jeffery, J. C.; McCleverty, J. A.; Ward, M. D. *Angew. Chem., Int. Ed.* **1998**, *37*, 1279. (c) Bell, Z. R.; Jeffery, J. C.; McCleverty, J. A.; Ward, M. D. *Angew. Chem., Int. Ed.* **2002**, *41*, 2515. (d) Paul, R. L.; Bell, Z. R.; Jeffery, J. C.; McCleverty, J. A.; Ward, M. D. *Proc. Natl. Acad. Sci. U.S.A.* **2002**, *99*, 4883. (e) Bell, Z. R.; Harding, L. P.; Ward, M. D. *Chem. Commun.* **2003**, 2432. (f) Argent, S. P.; Riis-Johannessen, T.; Jeffery, J. C.; Harding, L. P.; Ward, M. D. *Chem. Commun.* **2005**, 4647. (g) Argent, S. P.; Adams, H.; Riis-Johannessen, T.; Jeffery, J. C.; Harding, L. P.; Ward, M. D. *J. Am. Chem. Soc.* **2006**, *128*, 72. (h) Argent, S. P.; Adams, H.; Harding, L. P.; Ward, M. D. *Dalton Trans.* **2006**, 542. (i) Paul, R. L.; Argent, S. P.; Jeffery, J. C.; Harding, L. P.; Lynam, J. M.; Ward, M. D. *Dalton Trans.* **2004**, 3453.

(7) (a) Clegg, J. K.; Lindoy, L. F.; Moubaraki, B.; Murray, K. S.; McMurtrie, J. C. *Dalton Trans.* **2004**, 2417. (b) Eddaoudi, M.; Kim, J.; Wachter, J. B.; Chae, H. K.; O'Keeffe, M.; Yaghi, O. M. *J. Am. Chem. Soc.* **2001**, *123*, 4368. (c) Abrahams, B. F.; Egan, S. J.; Robson, R. *J. Am. Chem. Soc.* **1999**, *121*, 3535. (d) Mller, I. M.; Moller, D. *Angew. Chem., Int. Ed.* **2005**, *44*, 2969. (e) Haino, T.; Kobayashi, M.; Chikaraishi, M.; Fukazawa, Y.; *Chem. Commun.* **2005**, 2321.

(8) (a) Hasenknopf, B.; Lehn, J.-M.; Kneisel, B. O.; Baum, G.; Fenske, D. *Angew. Chem., Int. Ed. Engl.* **1996**, *35*, 1838. (b) Hasenknopf, B.; Lehn, J.-M.; Boumediene, N.; Dupont-Gervais, A.; van Dorsselaer, A.; Kneisel, B.; Fenscke, D. *J. Am. Chem. Soc.* **1997**, *119*, 10956. (c) Baum, G.; Constable, E. C.; Fenske, D.; Housecroft, C. E.; Kulke, T. *Chem. Commun.* **1999**, 195. (d) Tuna, F.; Hamblin, J.; Jackson, A.; Clarkson, G.; Alcock, N. W.; Hannon, M. J. *Dalton Trans.* **2003**, 2141. (e) Jones, P. L.; Byrom, K. J.; Jeffery, J. C.; McCleverty, J. A.; Ward, M. D. *Chem. Commun.* **1997**, 1361. (f) Mamula, O.; von Zelewsky, A.; Brodard, P.; Schlapfer, C. W.; Bernardinelli, G.; Stoeckli-Evans, H. *Chem.—Eur. J.* **2005**, *11*, 3049.

Scheme 1

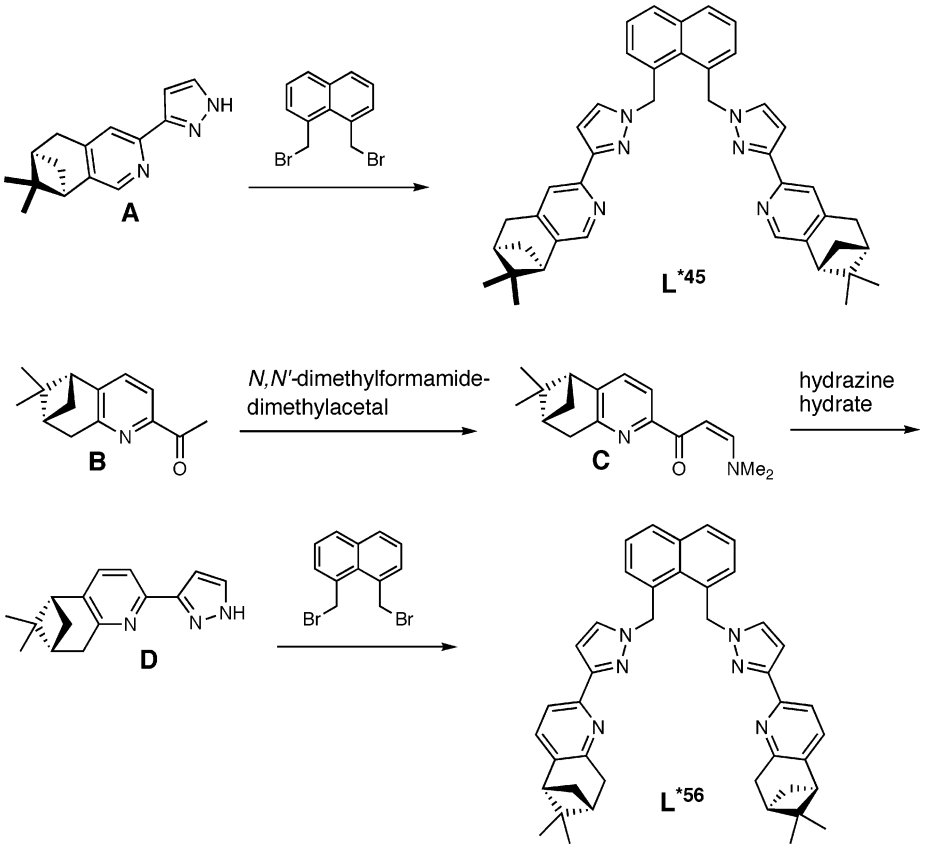

complexes $[M_8(L^{m-Ph})_{12}]^{16+}$,[6h] and a further change of the aromatic spacer to *p*-phenylene generates the largest homoleptic cages of this type that we have yet seen, the tetracapped truncated-tetrahedral cage complexes $[M_{16}(L^{p-Ph})_{24}]^{32+}$.[6g] In all cases, the requirement of the cages to have a 2:3 M−L ratio results in the formation of a cage structure in which the vertex−edge ratio is 2:3 (e.g., tetrahedron, 4:6; cube, 8:12), with a metal ion at each vertex and a bridging ligand spanning each edge. Thus, each edge-bridging ligand connects two metal ions, and each metal ion vertex is located at the meeting point of three edges, such that each ion receives three bidentate-coordinating units. The link between the stoichiometry of the complexes and the topologies of the cages is clear, and while we cannot predict the structure of the cage that will form with a given ligand, we can at least narrow down the range of possible cage topologies to a member of this set.

An additional interesting feature of some of these cages is their chirality, with $[M_4(L^{o-Ph})_6]^{8+}$ tetrahedra[6b,d] and $[M_{16}(L^{p-Ph})_{24}]^{32+}$ tetracapped truncated tetrahedra[6g] forming with all metal ions in one cage having the same trischelate chirality. This is necessary for the closed cages to form and means that, in (for example) $[M_{16}(L^{p-Ph})_{24}]^{32+}$, 96 metal−ligand bonds have to form with correct control of chirality during the assembly process. Crystals of these are, of course, racemic, containing equal amounts of the opposite cage enantiomers. If they could be resolved (using, e.g., a chiral anion such as "trisphat"[9]), they would make excellent "chiral containers" for enantioselective host−guest chemistry; however, the lability of the metal ions used for the self-assembly processes may render this a difficult exercise. An alternative approach to achieve a single enantiomer of a chiral assembly is to attach a chiral auxiliary to the ligand, such that the alternate enantiomers of the cages become diastereoisomers of different energy, and a single one may be preferred. Examples of the preparation of optically pure assemblies based on chiral ligands have been described by von Zelewsky[8f,10] and Constable,[11] and we also reported recently the diastereoselective preparation of a single isomer of an M_4L_6 tetrahedral cage based on L^{o-Ph}*, a chiral analogue of L^{o-Ph}.[6f]

We describe in this paper the coordination chemistry of the ligand L^{naph}, in which the two pyrazolyl−pyridine arms are connected by a 1,8-naphthalenediyl spacer. Again, a simple variation in the structure of the spacer compared to the other ligands in this series (Chart 1) results in a dramatic change in the structure of the coordination cages that are formed with M^{2+} ions, with a series of dodecanuclear cages having a truncated-tetrahedral topology being isolated. In addition, we describe the coordination behavior of L^{naph} with the monocations Cu^+ and Ag^+ and show how the structures of the complexes are highly anion-dependent, with either

(9) Lacour, J.; Hebbe-Viton, V. *Chem. Soc. Rev.* **2003**, *32*, 373

(10) (a) Mamula, O.; von Zelewsky, A. *Coord. Chem. Rev.* **2003**, *242*, 87. (b) Perret-Aebi, L. E.; von Zelewsky, A.; Dietrich-Buckecker, C. D.; Sauvage, J.-P. *Angew. Chem., Int. Ed.* **2004**, *43*, 4482.

(11) (a) Baum, G.; Constable, E. C.; Fenske, D.; Housecroft, C. E.; Kulke, T. *Chem.—Eur. J.* **1999**, *5*, 1862. (b) Baum, G.; Constable, E. C.; Fenske, D.; Housecroft, C. E.; Kulke, T.; Neuberger, M.; Zehnder, M. *J. Chem. Soc., Dalton Trans.* **2000**, 945.

simple mononuclear complexes or cyclic polynuclear helicates occurring depending on the nature of the counterion. Finally, we describe the syntheses of two chiral analogues of L^{naph} (L^{*45} and L^{*56}) in which pinene groups as chiral auxiliaries are fused to the pyridyl rings; their coordination chemistry provides some interesting examples of the extent to which the chiral auxiliaries can control the chirality of the metal−ligand assemblies that they form. This work follows that from a previous preliminary communication, which described the first dodecanuclear truncated-tetrahedral cage in this series.[6c]

Results and Discussion

Ligand Syntheses. Synthesis of the ligand L^{naph} was accomplished by reaction of 3-(2-pyridyl)pyrazole with 1,8-bis(bromomethyl)naphthalene and a base under phase-transfer conditions, using the standard method for ligands of this series; full details were given in the earlier communication.[6c] The chiral ligands L^{*45} and L^{*56}, based on von Zelewsky's "CHIRAGEN" series of ligands,[8f,10] were prepared in the same way from the appropriate chiral derivative of 3-(2-pyridyl)pyrazole. The 3-(2-pyridyl)pyrazole derivative with the pinene fused at positions C^4 and C^5 of the pyridyl ring (compound **A**, Scheme 1) was available from earlier work;[12] the isomer substituted at positions C^5 and C^6 of the pyridyl ring (compound **D**, Scheme 1) was prepared by conversion of the acetyl group of the known C^5/C^6-substituted 2-acetylpyridine[13] to a pyrazole group following a standard two-step procedure,[12,14] as shown in Scheme 1.

Complexes of the Achiral Ligand L^{naph} with Cu^I and Ag^I. Because L^{naph} is tetradentate, we would expect that its coordination to metal ions having a preference for four-coordinate geometries, viz., Cu^I and Ag^I, would result in the formation of complexes with a 1:1 metal−ligand ratio. This turned out to be the case, although the structures are strongly anion-dependent.

Reaction of L^{naph} with $[Cu(MeCN)_4](OTf)$ or $[Ag(MeCN)_4](BF_4)$ in MeCN, in a 1:1 ratio, afforded clear solutions from which crystals grew following slow diffusion of diethyl ether vapor into the solutions. The structures of the complexes so obtained are in Figures 1 and 2; both are relatively unremarkable mononuclear species in which both pyrazolyl−pyridine arms of L^{naph} coordinate to the sole metal ion. In $[Cu(L^{naph})](OTf)$, the four-coordinate Cu^I center has Cu−N separations in the range of 2.001−2.074 Å; the coordination geometry is, as is commonly the case, intermediate between planar and tetrahedral with an angle of 57° between the two CuN_2 planes. There is no close contact between the Cu^I center and the triflate anions. The gross structure of $[Ag(L^{naph})](BF_4)$ is generally similar, with the exceptions that (i) the two ligand arms are essentially coplanar, providing a planar array of four N-donor atoms around the Ag^I ion, and (ii) the Ag−N bonds fall into two sets, with two being short (both ca. 2.15 Å) and the other two being >2.7 Å, beyond the distance which would normally be considered to constitute a bond at all. However, we note that the pyridyl ring containing N(61) is oriented such that the N-donor atom is directed toward Ag(1), such that the coordination geometry is best described as linear two-coordinate Ag^I with two additional weak, long-range Ag···N interactions. Each molecule is bent into an "L" shape with an angle of 95° between the AgN_4 plane and the naphthyl unit; two of these are associated across an inversion center by an obvious π-stacking interaction.

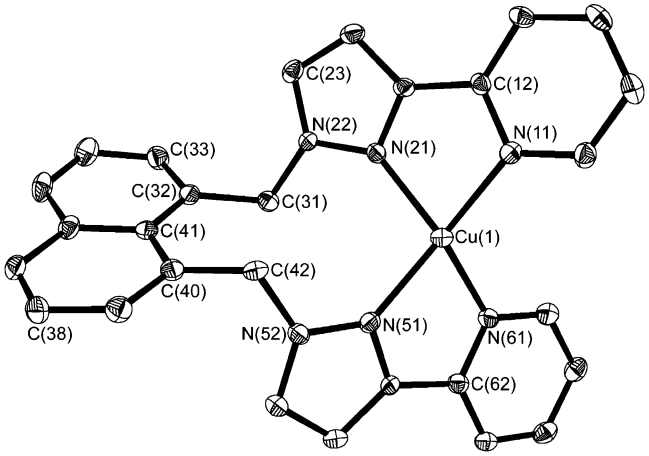

Figure 1. Structure of the complex cation of $[Cu(L^{naph})](OTf)$ showing thermal ellipsoids at the 40% probability level.

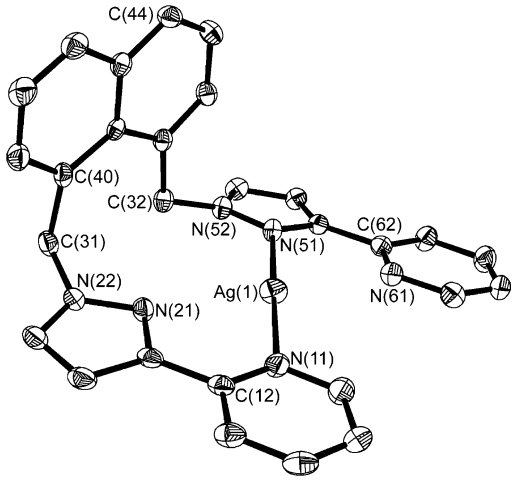

Figure 2. Structure of the complex cation of $[Ag(L^{naph})](BF_4)$ showing thermal ellipsoids at the 40% probability level.

Electrospray mass spectrometry (ESMS) spectra of these complexes in solution showed the presence of strong ions corresponding to the monocations $[M(L^{naph})]^+$, e.g., at *m*/*z* 505 for $\{Cu(L^{naph})\}^+$ and *m*/*z* 549 for $\{Ag(L^{naph})\}^+$. For $[Cu(L^{naph})](OTf)$, there was no evidence for the formation of higher-nuclearity species. However, for $[Ag(L^{naph})](BF_4)$, the ESMS spectrum also contained weaker signals at *m*/*z* 1187.2, 1825.0, and 2461.1, which correspond to traces of the oligomers $\{Ag_2(L^{naph})_2(BF_4)\}^+$, $\{Ag_3(L^{naph})_3(BF_4)_2\}^+$, and $\{Ag_4(L^{naph})_4(BF_4)_3\}^+$, respectively. Given the 1:1 metal−

(12) Motson, G. R.; Mamula, O.; Jeffery, J. C.; McCleverty, J. A.; Ward, M. D.; von Zelewsky, A. *J. Chem. Soc., Dalton Trans.* **2001**, 1389.
(13) Kolp, B.; Abeln, D.; Stoeckli-Evans, H.; von Zelewsky, A. *Eur. J. Inorg. Chem.* **2001**, 1207.
(14) (a) Amoroso, A. J.; Cargill Thompson, A. M. W.; Jeffery, J. C.; Jones, P. L.; McCleverty, J. A.; Ward, M. D. *J. Chem. Soc., Chem. Commun.* **1994**, 2751. (b) Bell, Z. R.; Motson, G. R.; Jeffery, J. C.; McCleverty, J. A.; Ward, M. D. *Polyhedron* **2001**, *20*, 2045.

ligand stoichiometry, the trimer and tetramer are likely to be circular helicates;[8] it is interesting that they appear (albeit as minor components) for $[Ag(L^{naph})](BF_4)$ but not $[Cu(L^{naph})](OTf)$, and this may suggest a templating role for the tetrafluoroborate anion. The ^1H NMR spectrum of $[Ag(L^{naph})](BF_4)$ was unremarkable, showing signals consistent with a single-ligand environment in 2-fold symmetry, consistent with the solid-state structure of the monomer. This suggests either that the higher oligomers are not present in sufficient quantity to show up clearly in the NMR spectrum or that there is fast exchange between several interconverting forms. Given the complexity of the structures, we feel that fast interconversion on the NMR time scale is unlikely, and indeed cooling the sample down did not result in a significant increase in the complexity of the ^1H NMR spectrum.

To see if tetrafluoroborate could act as a template for circular helicates in these systems, we also prepared the complex of L^{naph} with $[Cu(MeCN)_4](BF_4)$ in the same way. Diffusion of diethyl ether vapor into the reaction mixture resulted in the formation of crystals of $[Cu_4(L^{naph})_4][BF_4]_4$ in which four metal cations and four ligands have assembled into a cyclic helical array, with a tetrafluoroborate anion occupying the central cavity (Figure 3). All Cu^I ions are four-coordinate, from two pyrazolyl−pyridine units, with Cu−N distances in the range of 1.98−2.07 Å. The helical structure is a consequence of the four ligands having an "over-and-under" conformation around the complex, in contrast to a "face-to-face" array of two pairs of mutually perpendicular ligands, which would give a grid structure. There are three obviously favorable features of this structure. First, there is aromatic stacking between parallel ligand fragments around the periphery; each naphthyl unit is sandwiched between two pyridyl residues from adjacent ligands, giving four triple stacks around the complex. Second, the coordination geometry around each Cu^I is now as close to tetrahedral as possible given the constraints of the ligand bite angles, with the two bidentate pyrazolyl−pyridine units at each Cu^I center being essentially perpendicular (cf. 57° in the monomer because the two bidentate arms of one ligand cannot be mutually perpendicular). Third, the encapsulated fluoroborate anion is clearly a good fit for the center of the cavity. Its role as a template is confirmed by the fact that no such tetranuclear assembly occurs either in the solid state or in solution for the triflate complex, according to ESMS. In contrast, the ESMS spectrum of $[Cu_4(L^{naph})_4][BF_4]_4$ shows a sequence of peaks at *m*/*z* 2284.5, 1098.8, and 703.2, which correspond to the species $\{[Cu_4(L^{naph})_4][BF_4]_{4-x}\}^{x+}$ ($x = 1-3$) arising from sequential loss of tetrafluoroborate anions. Interestingly, a peak at *m*/*z* 1691.4 corresponds to the *trinuclear* species $\{[Cu_3(L^{naph})_3][BF_4]_2\}^+$, indicating that a mixture of cyclic trinuclear and tetranuclear species has formed in solution, with the tetranuclear species crystallizing preferentially. Such behavior has been observed by others in dynamically interconverting cyclic helical assemblies.[6c,d,f]

Complexes of the Achiral Ligand L^{naph} with Cu^{II}, Co^{II}, and Cd^{II}. Dodecanuclear Cages with a Truncated-Tetrahedral Topology. Upon prolonged standing in air, orange solutions of $[Cu_4(L^{naph})_4][BF_4]_4$ were observed to turn

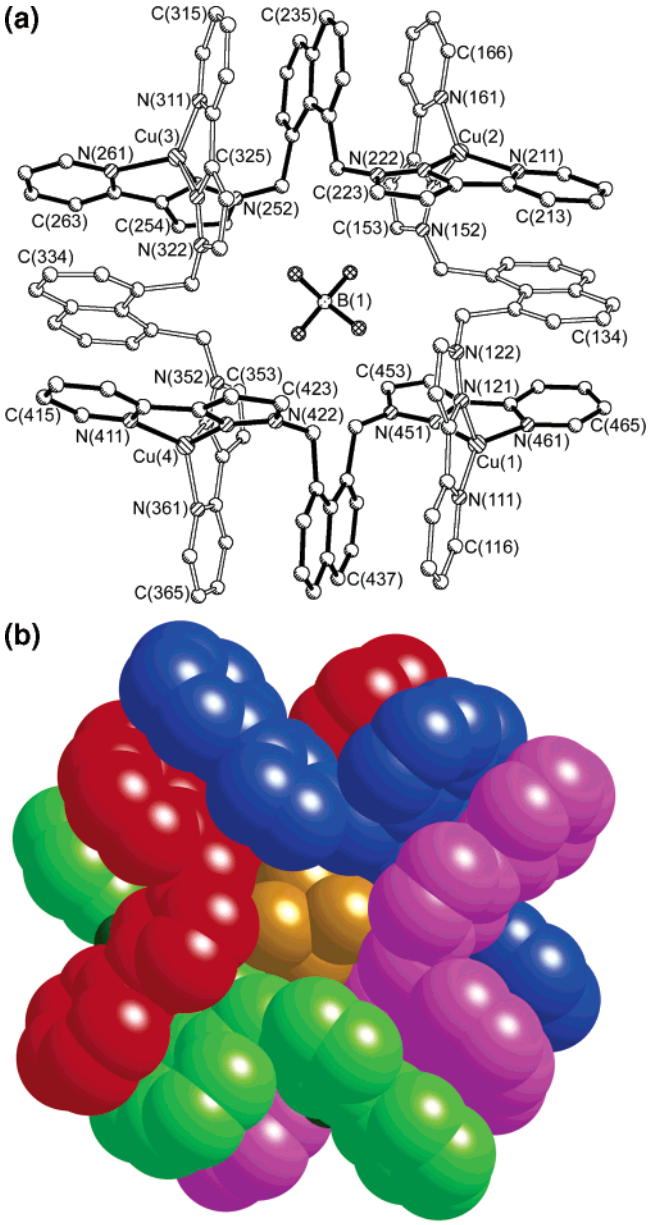

Figure 3. Two views of the complex cation of $[Cu_4(L^{naph})_4](BF_4)_4 \cdot 2MeCN \cdot {}^iPr_2O$: (a) a conventional view showing the labeling scheme, with alternating ligands shaded differently for clarity; (b) a space-filling picture showing atoms with their van der Waals radii (the four ligand strands are colored separately; the F atoms of the central fluoroborate anion are orange).

green, consistent with the formation of a Cu^{II} complex. We prepared a Cu^{II} complex directly by the reaction of L^{naph} with $Cu(ClO_4)_2$ in MeCN, followed by slow diffusion of diethyl ether vapor into the resulting green solution to precipitate crystals. The structure of the complex is shown in Figure 4; use of Cu^{II} rather than Cu^I, with the change in the M−L stoichiometry from 1:1 to 2:3 that ensues, has resulted in the formation of the dodecanuclear cage $[Cu_{12}(L^{naph})_{18}][(ClO_4)_{24}$, which has the topology of a truncated tetrahedron.

The structure can be considered to be derived from a parent tetrahedron, each of whose four vertices are sliced off to generate a triangular face (colored yellow in the figure). Each of the original triangular faces of our notional tetrahedron is now an approximate hexagon. The resulting truncated-tetrahedral structure has 12 vertices and 18 edges and thereby

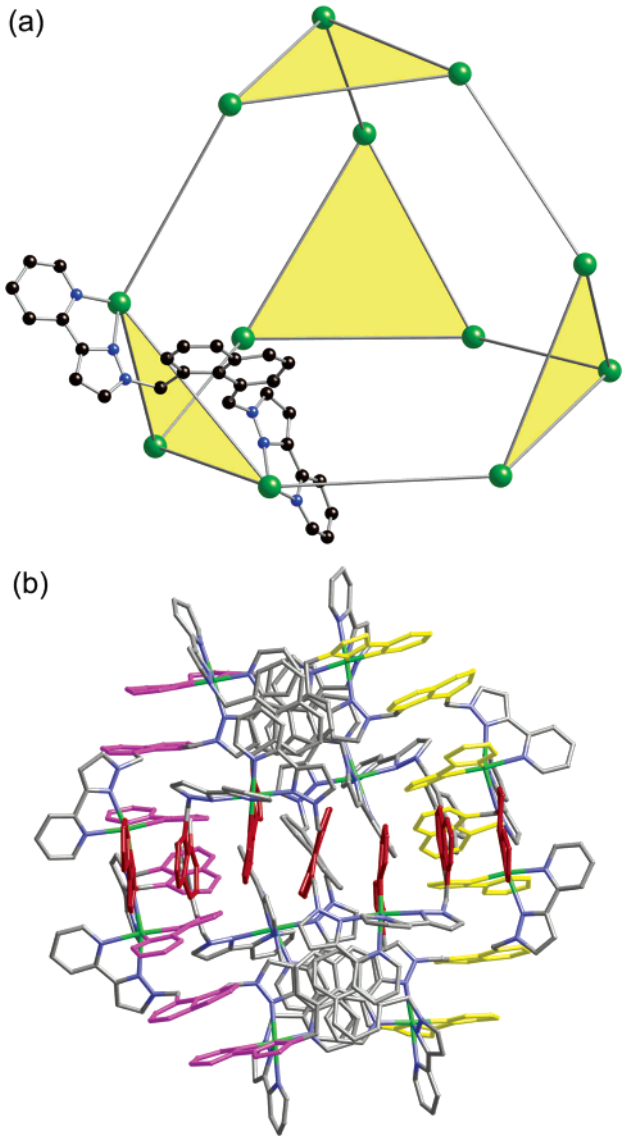

Figure 4. Two views of the complex cation of $[Cu_{12}(L^{naph})_{18}](ClO_4)_{24}\cdot 7.5MeCN$: (a) a view emphasizing the truncated-tetrahedral array of metal ions, with one bridging ligand shown (the faces colored yellow are those arising from truncation of the parent tetrahedron); (b) a view of the entire complex cation emphasizing the interligand aromatic stacking interactions, with three of the six sets of stacks colored in red, yellow, and purple.

matches the 2:3 M−L stoichiometric requirements of the Cu^{II}−L^{naph} combination, with a six-coordinate metal ion located at each vertex and a bridging ligand spanning each edge. The edges of the polyhedral cage (i.e., the shortest Cu···Cu separations) are in the range of 9.21−9.65 Å. There are two crystallographically independent cages in the unit cell, with each lying on a 3-fold rotation axis, such that the asymmetric unit contains two independent one-third cage fragments; i.e., there are eight independent Cu^{II} centers. All of the metal centers show the characteristic irregular coordination geometry of Jahn−Teller-distorted Cu^{II}. However, the distortion is not in the same sense in every case: Cu(1) and Cu(7) (one in each cage) show the more common elongation along one axis with four short and two long Cu−N distances, whereas the others all have two short and four long bonds, indicative of the more unusual axially compressed distortion. All Cu^{II} centers have a meridional arrangement of the three pyrazolyl−pyridine chelating ligands. The presence of a (noncrystallographic) 3-fold rotation axis through each of the four triangular faces means that each complex has approximate *T* symmetry; the chirality prevents adoption of higher symmetry such as T_d by removing the mirror planes. In a recent paper, Cotton et al. have pointed out that *T*-symmetric species may be derived by "downgrading" assemblies with tetrahedral, octahedral, or icosahedral symmetry by the removal of mirror planes,[15] and we have found (noncrystallographic) *T* symmetry to be surprisingly ubiquitous in our polynuclear cage assemblies.[6]

Several features of this structure are of particular note, in addition to the facts that it is unusual and attractive. (i) There is extensive aromatic stacking involving naphthyl and pyrazolyl−pyridine groups around the periphery of the complex; this is emphasized in Figure 4b. Seven-component stacks involving a sequence of alternating pyrazolyl−pyridine and naphthyl units from separate ligands are apparent, and this motif is repeated six times, with each 7-fold stack lying on one face of an approximate cube. (ii) The central cavity of the $[Cu_{12}(L^{naph})_{18}]^{24+}$ cage is large enough to accommodate four perchlorate anions. For the cage based on Cu(5)−Cu(8) and their symmetry equivalents, the four perchlorate anions form an approximately tetrahedral array with separations between the Cl atoms of approximately 5.6 Å (see Figure 5, which depicts the analogous Cd^{II} complex). The presence of relatively short CH···O contacts between ligands and perchlorate anions (nonbonded C···O separations down to 3.03 Å) suggests weak hydrogen-bonding interactions between the anions and those ligands which form the triangular faces of the cage. For the alternate cage, based on Cu(1)−Cu(4) and their symmetry equivalents, only three perchlorate anions (and one MeCN molecule) could be located in the cavity, but the severe disorder of the anions and weak diffraction means that not all anions could be located. (iii) There are also anions associated with the surface of the cage, sitting in the "windows" in the centers of the triangular faces of the cage (see Figure 5, which depicts the isostructural Cd^{II} complex) and also in pockets between pyridyl rings located along the six edges of the cage, which bridge the triangular faces. (iv) The structure is chiral, with all 12 metal trischelate centers in the cage having the same optical configuration. This is necessary for a closed cage to form; if the optical configuration at any metal center were inverted, then a ligand arm would end up directed outside the assembly and closure would not be possible. A consequence of this is that each triangular or pseudohexagonal face of the truncated tetrahedron has the three (or six) ligands arrayed between the metal ions in a cyclic helical motif (Figure 5).

Similar truncated-tetrahedral cage structures form with other combinations of metal cation and counteranion. Reaction of L^{naph} with $Co(BF_4)_2$ in the same way afforded $[Co_{12}(L^{naph})_{18}](BF_4)_{24}$, which has the same gross structure as $[Cu_{12}(L^{naph})_{18}](ClO_4)_{24}$, forming an approximate *T*-symmetry cage that accommodates four tetrafluoroborate anions in the central cavity (Figures 4 and 5). The only significant

(15) Cotton, F. A.; Murillo, C. A.; Yu, R. *Dalton Trans.* **2005**, 3161.

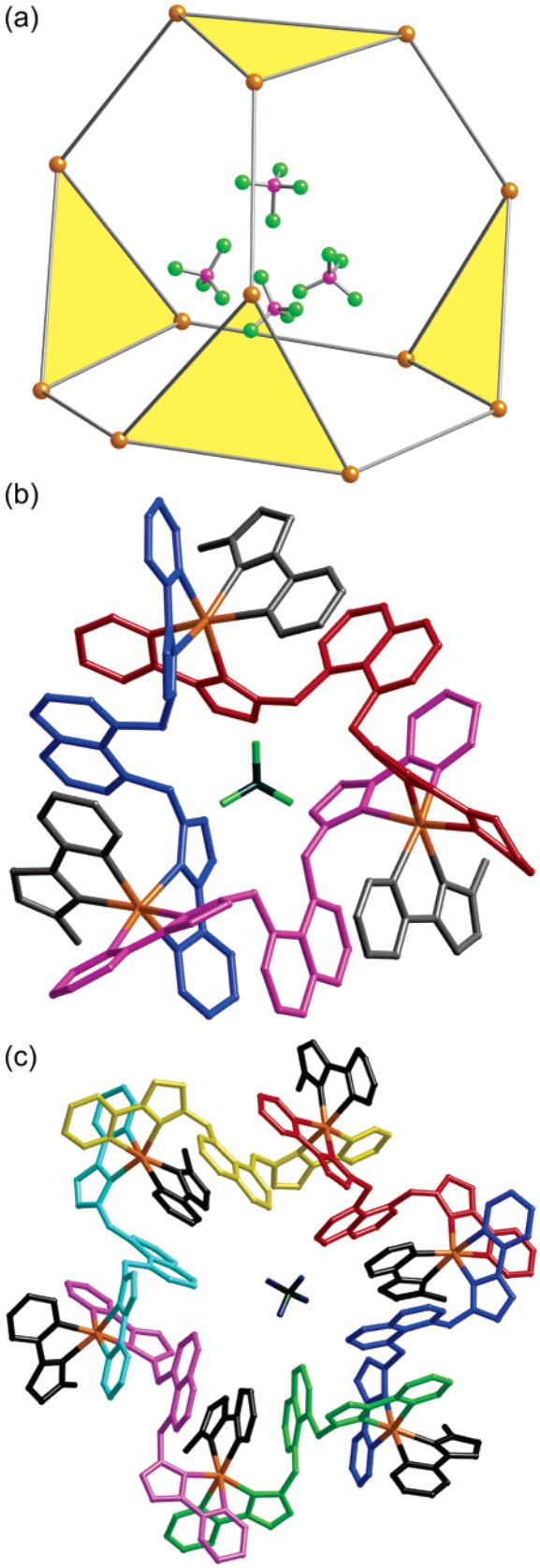

Figure 5. Three views of the structure of $[Cd_{12}(L^{naph})_{18}](BF_4)_{24}\cdot 6Et_2O\cdot 4.5MeCN\cdot 4H_2O$: (a) a view of the polyhedral metal cage and the four encapsulated $[BF_4]^-$ anions; (b) a view down one of the triangular faces, emphasizing the cyclic helical array of ligands around the face and the presence of an anion in the center of the face; (c) a view down one of the Cd_6 pseudohexagonal faces, emphasizing the cyclic helical array of ligands around the face and the presence of an anion in the center of the face.

difference between the two structures is that the Co^{II} ions have a more regular pseudooctahedral coordination geometry, with Co−N separations in the range of 2.1−2.2 Å, characteristic of high-spin Co^{II}. This structure was described in detail in our earlier communication and so is not discussed further here.[6c] We also prepared $[Cd_{12}(L^{naph})_{18}](BF_4)_{24}$ and found that the same cage structure can form with a larger second-row metal dication having Cd−N separations of 2.27−2.39 Å. Like the Cu^{II} complex, this crystallizes with two independent cages in the unit cell, each one lying on a 3-fold axis with four crystallographically unique metal ions. Despite the longer metal−ligand distances associated with a second-row metal ion, the Cd···Cd separations are in the range of 9.05−9.51 Å, similar to those observed for the Co^{II} and Cu^{II} cages. Both independent $[Cd_{12}(L^{naph})_{18}]^{24+}$ cages contain a tetrahedral array of four fluoroborate anions (B···B separations, 4.83−5.18 Å) and three MeCN molecules. These cages also feature the same arrangement of counterions in the triangular "windows" and along the six edges between the triangular faces that we saw in the Cu^{II} analogue. The arrangement of anions in the cavity and around the faces is emphasized for this complex in Figure 5.

The size of the cavity in these complexes may be estimated as follows. The shortest H···H separation across the "diameter" of the cavity is 9.6 Å. Subtracting the van der Waals radii (1.2 Å each) gives a spherical cavity of radius 3.6 Å and volume ≈200 Å; this is a low estimate because it does not allow for the elongation of the cavity toward the four windows in the hexagonal faces. A similar calculation reveals the diameter of these windows in the hexagonal faces to be ≈3.8 Å, sufficiently large to allow facile ingress and egress of small molecules. This accounts for the fact that ^{11}B NMR spectroscopy of $[Cd_{12}(L^{naph})_{18}](BF_4)_{24}$ in CD_3CN showed only a single resonance down to −40 °C, implying that the internal and external fluoroborate anions are in fast exchange. This contrasts with tetrahedral cages such as $[M_4(L^{o-Ph})_6]^{8+}$, in which the tightly bound anion is trapped on the NMR time scale,[6b,d] and the larger $[M_4(L^{biph})_6]^{8+}$, where exchange of internal and external anions could be frozen out in the NMR spectrum at low temperatures.[6i]

The three similar but subtly different structures show that the cage superstructure is robust and flexible enough to adapt itself to metal ions with different ionic radii (cf. Co vs Cd) and with varying degrees of distortion in their coordination sphere (cf. Cu vs Co), and we suggest that the extensive aromatic stacking between overlapping ligand fragments around the periphery of the complexes (Fig. 4b) plays a significant role in stabilizing the structure.

Retention of the cage complex structures in solution is shown by ESMS. In our original communication,[6c] we reported that we could not obtain evidence for the existence of $[Co_{12}(L^{naph})_{18}](BF_4)_{24}$ in solution by ESMS. However, by using relatively concentrated solutions (2 mg/mL) in MeCN and under mild conditions (see Experimental Section), we could obtain good mass spectra of the two new cages. The ESMS spectrum of $[Cu_{12}(L^{naph})_{18}](ClO_4)_{24}$ showed intense peaks at *m*/*z* 604 and 473.6, corresponding to mononuclear species $\{Cu(L^{naph})(ClO_4)\}^+$ and $\{CuL_2\}^{2+}$, respectively,

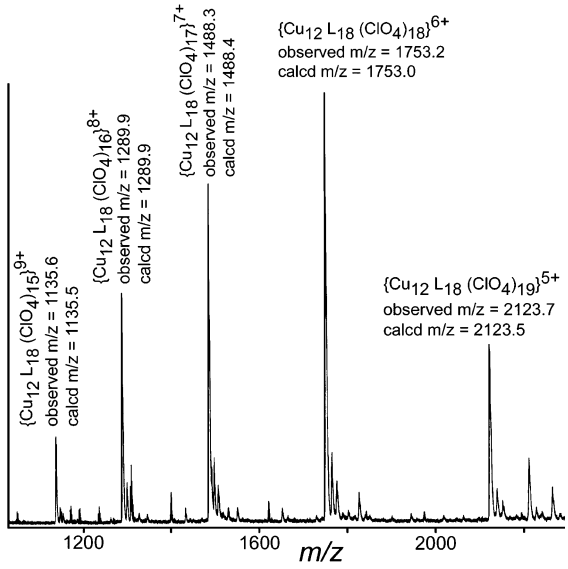

Figure 6. Part of the ESMS spectrum of $[Cu_{12}(L^{naph})_{18}](ClO_4)_{24}$ in the high *m*/*z* range (>1000), illustrating the sequence of peaks corresponding to the intact cage in solution associated with different numbers of counterions. The calculated *m*/*z* values are based on the most intense component of the isotope envelope.

which must arise from either some dissociation of the cage in solution or fragmentation in the mass spectrometer. However, at higher *m*/*z* values, a less intense sequence of peaks at *m*/*z* 2123.7, 1753.2, 1488.3, 1289.9, and 1135.6 was observed, which correspond to the species $\{[Cu_{12}(L^{naph})_{18}](ClO_4)_{24-x}\}^{x+}$ ($x = 5-9$, respectively) formed by sequential loss of perchlorate anions from the intact cage assembly (Figure 6). The ESMS spectrum of $[Cd_{12}(L^{naph})_{18}](BF_4)_{24}$ showed a very similar sequence of peaks at *m*/*z* 2762.9, 2192.9, 1812.4, 1541.1, 1337.8, and 1180.2, corresponding to the species $\{[Cd_{12}(L^{naph})_{18}](BF_4)_{24-x}\}^{x+}$ ($x = 4-9$, respectively). These cages therefore retain their integrity to some extent in solution and are not just artifacts of crystallization. This is important because it means that the cages may be able to show interesting host−guest chemistry with other anions in solution; the possibility of using larger anions that may be trapped in the central cavities is particularly interesting.

The truncated tetrahedron, which is the simplest of the Archimidean solids,[1c] is a very rare topology for coordination cages. Robson and co-workers have described how four trinuclear, triangular complexes assemble by hydrogen bonding to give a truncated-tetrahedral array of 12 Cd^{II} centers,[16] and $[Sn_{12}]^{12-}$ clusters with this topology have recently been reported to occur in the Zintl compounds $SrNa_{10}Sn_{12}$ and $CaNa_{10}Sn_{12}$.[17] In addition, Stang and co-workers have recently reported a series of complexes described as truncated tetrahedra,[5b,e] which are rather simpler M_6L_4 systems containing six metal vertexes in an octahedral array with four triangular ligands occupying half of the faces. This topology is identical with that of Fujita's well-known M_6L_4 cage,[3a−c] which is often described as "octahedral" (because of the arrangement of metal vertexes) even though it really has tetrahedral symmetry.

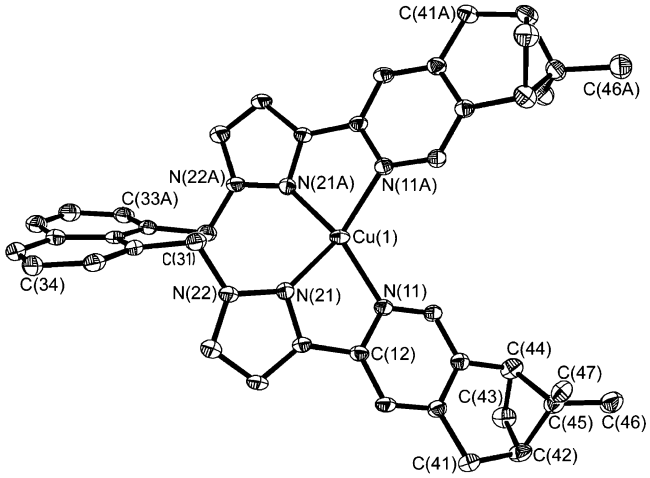

Figure 7. Structure of the complex cation of $[Cu(L^{*45})](BF_4)\cdot MeCN$ showing thermal ellipsoids at the 40% probability level.

Complexes of the Chiral Ligands L*[45] and L*[56] with Cu^I and Ag^I. Reaction of L^{*45} with $[Cu(MeCN)_4][BF_4]$ in MeCN, followed by slow crystallization of the reaction mixture, afforded crystals that we expected to be a tetranuclear cyclic helicate analogous to $[Cu_4(L^{naph})_4][BF_4]_4$. However, the crystals proved to be mononuclear $[Cu(L^{*45})](BF_4)$ (Figure 7), in which the chiral ligand coordinates as a tetradentate chelate in a manner similar to that observed for $[Cu(L^{naph})](OTf)$. The complex crystallizes in the chiral space group $C222_1$ and lies on a 2-fold rotation axis; the Cu^I ion is in an unremarkable pseudotetrahedral coordination environment with an angle between the two CuN_2 planes of 50°.

ESMS, however, revealed that the solution behavior is more complicated: in addition to peaks at *m*/*z* 693.0 and 346.5 for the monomer $\{Cu(L^{*45})\}^{n+}$ ($n = 1$ and 2), peaks were also observed at *m*/*z* 1562.2 and 1083.4, corresponding to the dinuclear species $\{Cu_2(L^{*45})_2(BF_4)_2\}^+$ and trinuclear species $\{Cu_3(L^{*45})_3(BF_4)\}^{2+}$, respectively. Some aggregation into higher-nuclearity oligomers is therefore occurring, although we could find no evidence for the anticipated tetramer. A possible explanation for this may be the steric crowding caused by the bulky pinene groups on the pyridyl rings, which would interfere with the pyridyl−naphthyl−pyridyl stacks apparent in the structure of $[Cu_4(L^{naph})_4][BF_4]_4$ (see Figure 3).

$[Ag(L^{*45})](ClO_4)$ has a very similar mononuclear structure (Figure 8), with the ligand being a tetradentate chelate having a twist angle of 52° between the two AgN_2 planes; in this case, all four N-donor atoms are fully coordinated, in contrast to the behavior shown by $[Ag(L^{naph})](BF_4)$, which was essentially two-coordinate (see earlier). As with $[Cu(L^{*45})](BF_4)$, however, the solution behavior of $[Ag(L^{*45})](ClO_4)$ is more complicated, with ESMS revealing the presence of a series of (presumably cyclic) oligomers (Figure 9a). The mass spectrum showed a strong peak at *m*/*z* 739 for monomeric $\{Ag(L^{*45})\}^+$ and weaker peaks at *m*/*z* 1576.2 for dimer $\{Ag_2(L^{*45})_2(ClO_4)\}^+$, *m*/*z* 2415.0 for trimer $\{Ag_3(L^{*45})_3(ClO_4)_2\}^+$, *m*/*z* 3253.3 for tetramer

(16) Müller, I. M.; Robson, R.; Separovic, R. *Angew. Chem., Int. Ed.* **2001**, *40*, 4385.
(17) Bobev, S.; Sevov, S. C. *Inorg. Chem.* **2001**, *40*, 5361.

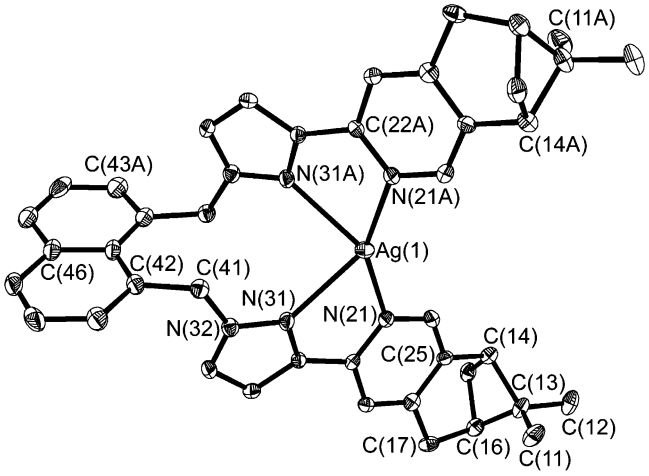

Figure 8. Structure of the complex cation of $[Ag(L^{*45})](ClO_4)\cdot MeCN$ showing thermal ellipsoids at the 40% probability level.

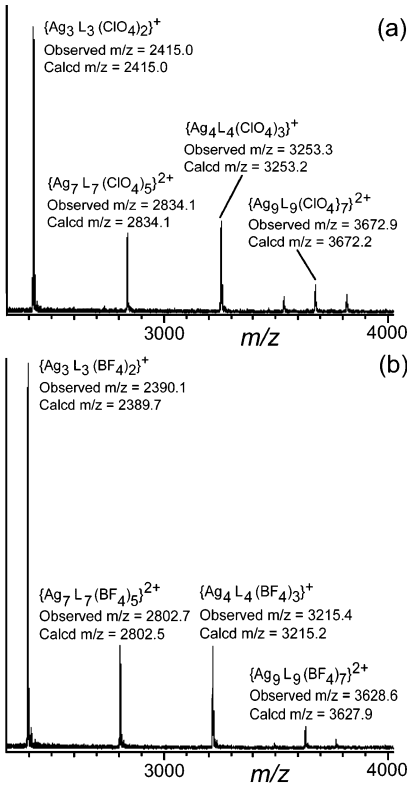

Figure 9. Parts of the ESMS spectra in the high *m*/*z* range (>2000) of (a) $[Ag(L^{*45})](ClO_4)$ and (b) $[Ag_4(L^{*56})_4](BF_4)_4$ in MeCN, illustrating the similarity of their solution behavior despite their different stoichiometries in the crystalline state. The calculated *m*/*z* values are based on the most intense component of the isotope envelope. The charges for these species (1+ or 2+) were all confirmed by the spacings between the isotope components, which were 1 or 0.5 mass units, respectively.

$\{Ag_4(L^{*45})_4(ClO_4)_3\}^+$, and also at *m*/*z* 2834.1 and 3672.9, which we tentatively ascribe to heptamer $\{Ag_7(L^{*45})_7(ClO_4)_5\}^{2+}$ and nonamer $\{Ag_9(L^{*45})_9(ClO_4)_7\}^{2+}$, respectively. Although the mononuclear species dominates (according to the ESMS spectrum), an extensive series of cyclic oligomers form as minor components in solution; attempts to crystallize these were unsuccessful, with all crystals isolated being of the monomer.

Using the alternate chiral ligand L^{*56} gave us more success in the structural characterization of cyclic helicates containing

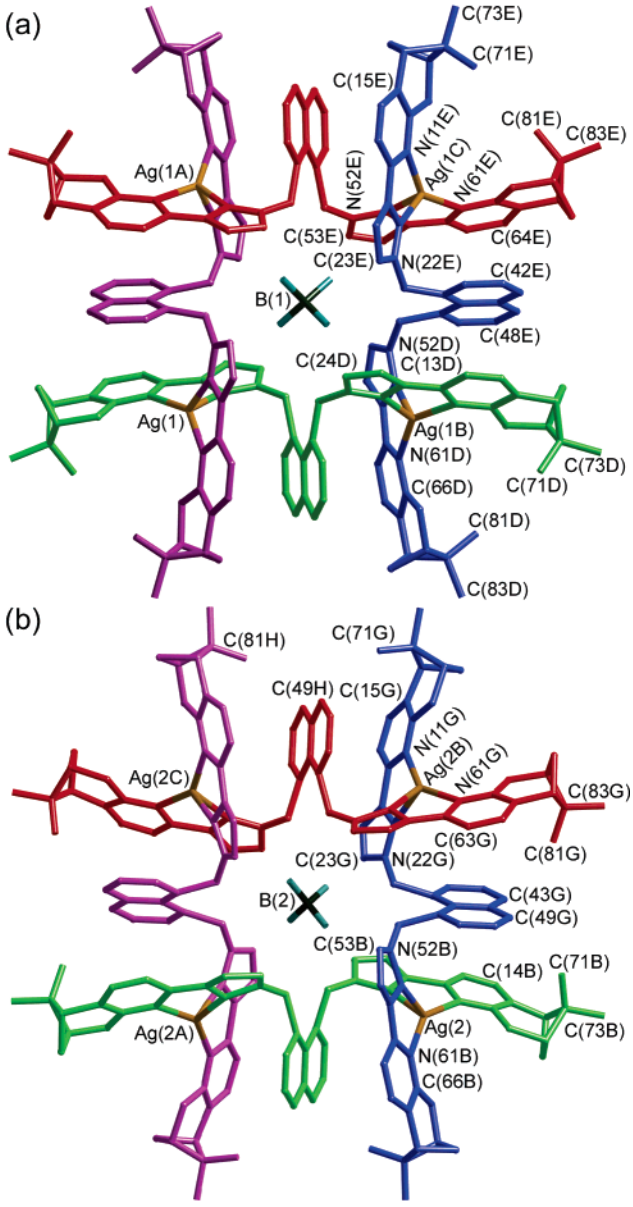

Figure 10. Structures of the two independent complex cations (different diastereomers) of $[Ag_4(L^{*56})_4](BF_4)_4\cdot(H_2O)_{0.5}$ with the ligands colored independently for clarity.

a chiral auxiliary. In principle, this ligand is expected to be better suited than L^{*45} for imparting chirality to complexes with tetrahedrally coordinated metals because the chiral groups must necessarily be closer to the metal center and will therefore exert a stronger influence on the metal coordination environment, specifically the sense of helicity associated with coordination of the bidentate pyrazolyl−pyridine groups. Reaction of L^{*56} with $[Ag(MeCN)_4][BF_4]$ in MeCN in a 1:1 proportion, followed by slow crystallization of the reaction mixture, afforded crystals of the cyclic tetranuclear helicate $[Ag_4(L^{*56})_4](BF_4)_4$ (Figure 10). The general topology is identical with that seen earlier in $[Cu_4(L^{naph})_4][BF_4]_4$ (Figure 3), with four bisbidentate bridging ligands spanning the edges of a square with a Ag^I ion at each corner and each naphthyl group sandwiched between two pyrazolyl−pyridine groups along each edge of the

complex. A disordered BF_4^- anion occupies the central cavity.

The complex crystallizes in the chiral space group *P*4, and the unit cell contains two independent cyclic helicates (Figure 10). Unexpectedly, these turn out to be diastereoisomers, with opposite senses of helical chirality but the same chirality in the pinene groups. The two diastereosiomers have significantly different overall sizes, with the Ag···Ag separation of 8.27 Å in one diastereoisomer [containing Ag(1)] being significantly shorter than that in the other one (8.90 Å). The Ag−N bond distances are in the same range in each case, 2.3−2.4 Å.

The origins of the structural differences between the two diastereomeric helicates can be seen to arise from steric effects associated with the orientation of the pinene groups. In one case [the helicate containing Ag(1)], the bulkier face of the pinene group is directed away from the naphthyl spacer, toward the corner of the complex. The two pinene groups associated with each Ag(1) center do not get in each other's way, with the closest nonbonded C···C interaction, between C(71) of one ligand and C(81) of the next, being 5.67 Å. This diastereomer is therefore relatively unhindered, and the Ag···Ag separation of 8.27 Å is not much longer than the Cu···Cu separations observed in $[Cu_4(L^{naph})_4][BF_4]_4$. The two AgN_2 planes at each Ag(1) center have an angle of 79° between them. In the alternate diastereomer [containing Ag(2)], the bulkier faces of the pinene units face each other along one edge of the square, such that one of the methyl groups is directed toward the naphthyl unit at the center of the sandwich, resulting in close pinene−naphthyl contacts: for example, the separation between C(81) of the pinene group on one ligand and C(49) of the naphthyl group toward which it is directed is only 3.43 Å. This results in the two pyridine units being pushed apart from one another toward the corners of the complex, with their planes now diverging at an angle of 25° [cf. 13° for the alternate diastereomer containing Ag(1)]. This has two consequences. First, the stacking interactions between the pyridyl−pyrazole units and the naphthyl units are compromised. Second, the coordination geometry around the Ag^I ions is significantly distorted, with the angle between the two AgN_2 planes being compressed to 68°. The steric strain results in a significantly longer Ag···Ag separation of 8.90 Å compared to that of the other diastereomer.

Clearly, we would not expect the two diastereomers to be present to the same extent at equilibrium; the presence of unfavorable steric interactions in the Ag(2) diastereomer suggests that this should be the minor component. ^{1}H NMR spectroscopy, however, was unhelpful because the spectra were broad even when the sample was cooled, preventing detection and integration of the signals for the two diastereomers. This is likely to be due to dynamic interconversion between cyclic oligomers of different sizes on the NMR time scale. ESMS confirmed that, again, the solution behavior is much more complicated than the solid-state behavior. The ESMS spectrum (Figure 9b) showed peaks at *m*/*z* 739 [monomer $\{Ag(L^{*56})\}^+$], *m*/*z* 1576.3 [dimer $\{Ag_2(L^{*56})_2(BF_4)\}^+$], *m*/*z* 2390.1 [trimer $\{Ag_3(L^{*56})_3(BF_4)_2\}^+$], *m*/*z* 3215.4 [tetramer $\{Ag_4(L^{*56})_4(BF_4)_3\}^+$], *m*/*z* 2802.7 [heptamer $\{Ag_7(L^{*56})_7(BF_4)_5\}^{2+}$], and *m*/*z* 3628.6 [nonamer $\{Ag_9(L^{*56})_9(BF_4)_7\}^{2+}$]; the presence of peaks corresponding to 7- and 9-mer species is exactly consistent with what we observed in the ESMS spectrum of redissolved crystals of the mononuclear complex $[Ag(L^{*45})](ClO_4)$, with the isomeric ligand and a different counterion. Even though $[Ag(L^{*45})](ClO_4)$ and $[Ag_4(L^{*56})_4](BF_4)_4$ crystallize as monomer and tetramer, respectively, their behavior in solution is clearly similar.

Tetrahedral Cage Complex of the Chiral Ligand L*^{45} with Zn^{II}. Following the successful characterization of a tetranuclear cyclic helicate containing a chiral auxiliary on the ligand, we were interested to see if L^{*45} or L^{*56} would form, upon reaction with M^{2+} cations, a dodecanuclear truncated-tetrahedral cage analogous to $[M_{12}(L^{naph})_{18}]^{24+}$ described above (M = Co, Cu, Cd) but as a single diastereomer.

We were unable to isolate any products from the reaction of M^{2+} salts with L^{*56}. The steric bulk of the pinene groups close to the metal coordination site seems to be too great to allow stable trischelate complexes to form, which is not surprising. Numerous derivatives of 2,2′-bipyridine and 1,10-phenanthroline with substituents immediately adjacent to the N donors are known, but they generally give stable complexes only with pseudotetrahedral cations such as Ag^I or Cu^I where the two ligands are mutually orthogonal and the substituents can avoid each other.

However, the reaction of $Zn(ClO_4)_2$ with L^{*45} (2:3 ratio) in MeCN afforded, upon crystallization of the reaction mixture, crystals of a complex that proved, unexpectedly, to be the tetrahedral cage $[Zn_4(L^{*45})_6](ClO_4)_8$, with a metal ion at each vertex of the tetrahedron and a bridging ligand spanning each of the six edges (Figure 11). This complex crystallizes in the chiral space group $F4_132$ with only $^1/_{12}$ of the complex in the asymmetric unit, with the rest of the complex being generated by a combination of 3- and 2-fold rotations. There is a (disordered) perchlorate anion in the central cavity. Like the related complex $[Zn_4(L^{o-Ph*})_6](BF_4)_8$ that we described recently,[6f] based on a shorter ligand with an *o*-phenylene spacer, a single enantiomer of $[Zn_4(L^{*45})_6](ClO_4)_8$ has formed in which the chirality of the pinene groups on the ligand dictates the sense of the chirality of the six metal trischelate units (which are homochiral). It is clear from the view looking down a C_3 axis that this arrangement minimizes steric interactions between the pinene groups, which are close together because of the *fac* trischelate geometry at each metal center. The complex has (crystallographic) *T* symmetry. Interestingly, and rather surprisingly, the optical configuration of the four metal trischelate centers is opposite to that observed in the crystal structure of $[Zn_4(L^{o-Ph*})_6](BF_4)_8$,[6f] despite the same configuration of the pinene groups.

Despite the slightly greater separation between the pyrazolyl−pyridine binding sites of L^{*45} compared to those of L^{o-Ph} and L^{o-Ph*}, afforded by a 1,8-naphthyl spacer instead of a 1,2-phenylene spacer, the Zn···Zn separations of 9.8 Å are about the same in $[Zn_4(L^{*45})_6](ClO_4)_8$ as they are in the

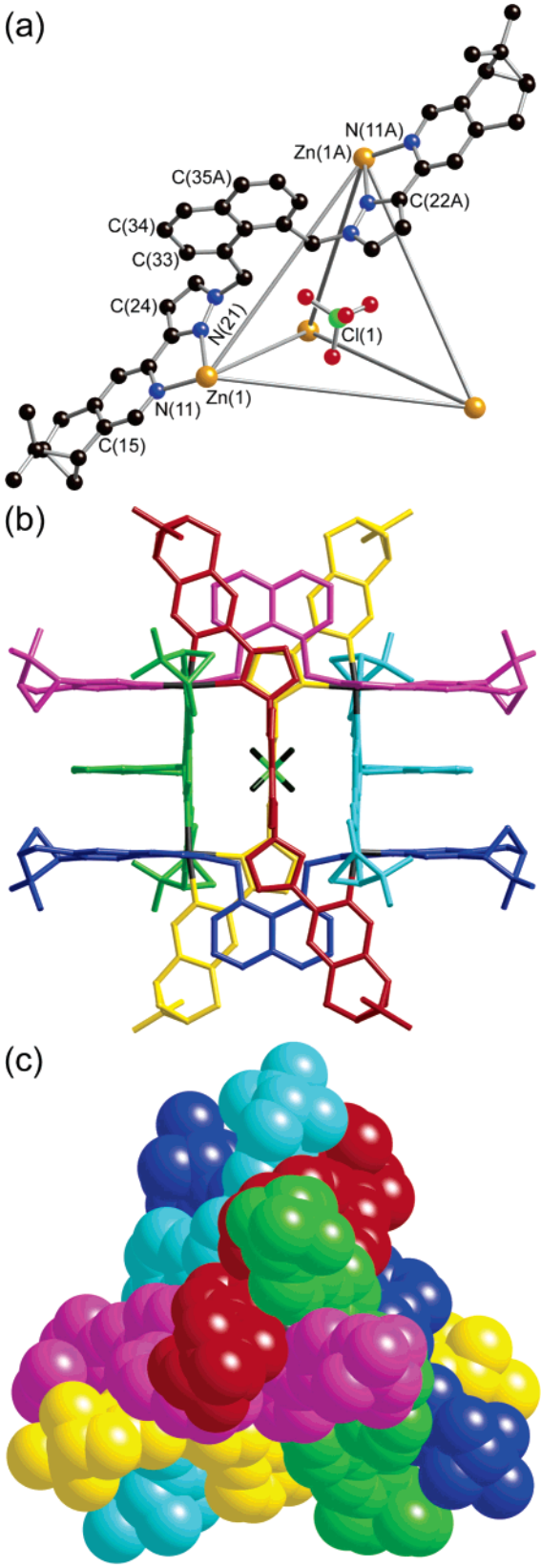

Figure 11. Three views of the structure of $[Zn_4(L^{*45})_6](ClO_4)_8$: (a) a view emphasizing the tetrahedral metal array, showing one bridging ligand and the encapsulated anion; (b) a view of the whole cage assembly with each ligand colored differently, emphasizing the aromatic stacking between ligands; (c) a space-filling view looking down one of the C_3 axes.

analogous complexes with L^{o-Ph} and L^{o-Ph*}.[6b,f] Each naphthyl unit is involved in stacking interactions with the two pyrazolyl−pyridine units on either side; the three components of the stack are substantially offset, with some H atoms of one aromatic unit lying above the π clouds of the next. The perchlorate guest is inverted with respect to the Zn_4 tetrahedron such that each O atom is directed toward the center of a triangular face of the cage. The O atoms are involved in CH···O hydrogen-bonding interactions[18] with atoms H(31) (on the methylene spacers), which are directed into the cavity; the relevant parameters are as follows: O(1)···C(31), 3.30 Å; O(1)···H(31), 2.69 Å; C−H···O angle, 120.5°. The high symmetry of the cage means that there are 12 such interactions between the perchlorate anion and the cage superstructure.

ESMS and ^{1}H NMR spectroscopy both confirm that the cage retains its integrity to a large extent in solution. The ESMS spectrum shows a sequence of strong peaks at *m*/*z* 1107.2, 1509.4, and 2313.9, which correspond to $\{Zn_4(L^{*45})_6(ClO_4)_{8-n}\}^{n+}$ (n = 4, 3, 2, respectively), i.e., arising from the intact complex with loss of 2, 3, or 4 perchlorate counterions. Intriguingly, however, there is also a much weaker series of peaks [<5% of the intensity of the weakest of the three peaks for $\{Zn_4(L^{*45})_6(ClO_4)_{8-n}\}^{n+}$] at *m*/*z* 1970.8, 2796.7, and 3523.1, which correspond to $\{Zn_{12}(L^{*45})_{18}(ClO_4)_{24-n}\}^{n+}$ (n = 7, 5, 4, respectively), i.e., the initially expected dodecanuclear truncated-tetrahedral cage. [The expected peak for the 6+ species $\{Zn_{12}(L^{*45})_{18}(ClO_4)_{18}\}^{6+}$ is obscured by the much stronger peak corresponding to $\{Zn_4(L^{*45})_6(ClO_4)_6\}^{2+}$, which has an identical value of *m*/*z* 2314]. Thus, $[Zn_{12}(L^{*45})_{18}](ClO_4)_{24}$ does form to a small extent in solution, but the simpler complex $[Zn_4(L^{*45})_6](ClO_4)_8$ substantially dominates and is the one that crystallizes. Steric factors clearly play an important role here. In the dodecanuclear cages, the trischelate metal centers all have a *meridional* arrangement of ligands, whereas in the simpler tetrahedral cage, all of the metal trischelates are *facial*. Although a *meridional* arrangement results in the bulky groups being further apart from one another and is usually preferred in simple mononuclear complexes of asymmetric bidentate ligands,[19] in the dodecanuclear cage structure, the bulk of the pinene groups would disrupt the extensive aromatic stacking between ligands and would result in other unfavorable interligand interactions [cf. the structure of $[Ag_4(L^{*56})_4](BF_4)_4$ discussed earlier]. Although this does not preclude completely the formation of $[Zn_{12}(L^{*45})_{18}](ClO_4)_{24}$, it destabilizes it relative to $[Zn_4(L^{*45})_6](ClO_4)_8$, where the pinene groups can be accommodated at the periphery of the complex away from the highly congested center thanks to the *facial* trischelate arrangement of the ligands. Clearly, entropic factors could also be important in the formation of dodcanuclear vs tetrahedral cages, but in the absence of hard evidence, we prefer not to speculate further on this point at the moment.

(18) (a) Desiraju, G.; Steiner, T. *The weak hydrogen bond in structural chemistry and biology*; OUP: Oxford, U.K., 1999. (b) Desiraju, G. R. *Chem. Commun.* **2005**, 2995.
(19) Fletcher, N. C.; Nieuwenhuyzen, M.; Rainey, S. *J. Chem. Soc., Dalton Trans.* **2001**, 2641.

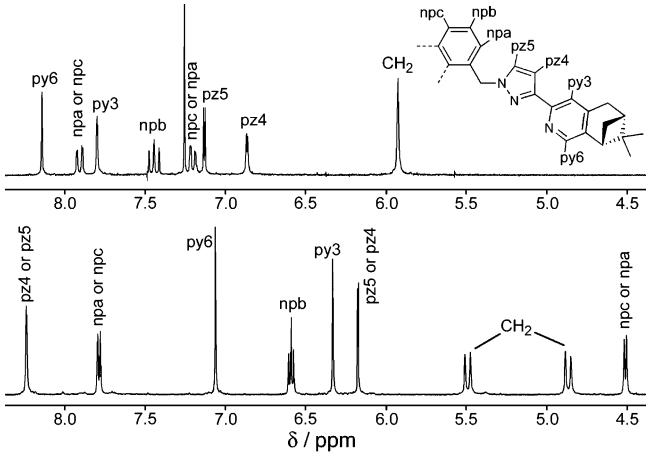

Figure 12. 500-MHz ^{1}H NMR spectra (4−9 ppm region only) of (top) L^{*45} in $CDCl_3$ and (bottom) $[Zn_4(L^{*45})_6](ClO_4)_8$ in CD_3CN.

The ^{1}H NMR spectrum of redissolved crystals of $[Zn_4(L^{*45})_6](ClO_4)_8$ (Figure 12) is consistent with the solid-state structure; we can assume that the trace amounts of $[Zn_{12}(L^{*45})_{18}](ClO_4)_{24}$ do not contribute significantly and that the spectrum observed is essentially that of $[Zn_4(L^{*45})_6](ClO_4)_8$. The spectrum shows the expected number of signals for the tetrahedral cage in which all ligands are equivalent and each has 2-fold symmetry. Substantial upfield shifts (compared to the free ligand) associated with some of the naphthyl and pyridyl protons are consistent with the aromatic stacking observed in the solid state; for example, one of the naphthyl resonances shifts to 4.5 ppm, and pyridyl H^3 shifts to 6.3 ppm. Also worth noting is the pair of doublets at 4.8 and 5.5 ppm arising from the diastereotopic CH_2 protons in a chiral environment. Significantly, there is no evidence for a second set of peaks associated with a different diastereomer, so we can see that the control of complex chirality imposed by the ligand is effective in this case [in notable contrast to $[Ag_4(L^{*56})_4](BF_4)_4$, with a single diastereomer being formed.

Conclusions

This set of bisbidentate ligands based on a 1,8-naphthyl spacer has generated some interesting coordination chemistry. L^{naph} can form 1:1 metal−ligand complexes with Cu^I and Ag^I and 2:3 complexes with Co^{II}, Cu^{II}, and Cd^{II}. The 1:1 complexes may be simple mononuclear species (with the ligand acting as a tetradentate chelate) or a cyclic helicate (in which the ligands are bridging), depending on whether the anion present can template the formation of the cyclic helicate; traces of other cyclic oligomers are present in solution. The 2:3 complexes with Co^{II}, Cu^{II}, and Cd^{II} are actually chiral $[M_{12}(L^{naph})_{18}]^{24+}$ cages, which consist of a truncated-tetrahedral array of metal ions with a bridging ligand spanning each of the 18 edges of the polyhedron; the central cavity is large enough to accommodate four anions. Extensive aromatic π stacking between pyrazolyl−pyridine and naphthalene units around the periphery of the complex is a feature of all of these cages. The sequence of complexes formed with Cu is particularly interesting: mononuclear $[Cu^I(L^{naph})]^+$ converts to the tetranuclear cyclic helicate $[Cu^I_4(L^{naph})_4]^{4+}$ in the presence of tetrafluoroborate as a templating anion; use of Cu^{II}, however, generates $[Cu_{12}(L^{naph})_{18}]^{24+}$. This constitutes an appealing series of structures of increasing complexity (mononuclear, cyclic tetranuclear helicate; dodecanuclear truncated tetrahedron) as a result of differences in the nature of the anion and metal oxidation state during the self-assembly process.

Complexes with analogous chiral ligands L^{*45} and L^{*56} have also been prepared. The complexes with Cu^I and Ag^I show the same general behavior, with 1:1 mononuclear complexes or 4:4 cyclic helicates being the dominant structures; the chirality of the ligand is not sufficient to dictate completely the chirality of the cyclic helicate, with a mixture of diastereoisomers present in the crystal structure of $[Ag_4(L^{*56})_4](BF_4)_4$. Reaction of L^{*45} with $Zn(ClO_4)_2$ afforded, unexpectedly, the tetrahedral cage $[Zn_4(L^{*45})_6](ClO_4)_8$ as a single diastereoisomer rather than the dodecanuclear cage $[Zn_{12}(L^{*45})_{18}](ClO_4)_{24}$, which only exists in solution as a minor product; this can be explained on steric grounds. The perchlorate anion in the central cavity of $[Zn_4(L^{*45})_6](ClO_4)_8$ interacts with the surrounding ligands via a network of CH···O hydrogen bonds.

The host−guest chemistry of these cages, and their luminescence associated with the naphthyl groups in the ligands, is currently under investigation.

Experimental Section

General Procedures. L^{naph} (ref 6c) and 3-(2′-pinene[4′,5′]-pyridyl)pyrazole (Scheme 1, compound **A**)[12] were prepared according to the previously described methods. ^{1}H NMR spectra were recorded on Bruker AC-250 or AMX2-400 spectrometers. Electron impact mass spectra were recorded on a VG-Autospec magnetic sector instrument. ESMS spectra were measured on a Bruker MicroTOF instrument in positive ion mode, with capillary exit and first skimmer voltages of 30 and 60 V, respectively. Samples were prepared at a concentration of ca. 2 mg/mL in MeCN and analyzed by direct infusion using a Cole-Parmer syringe pump at a flow rate of 3 mL/min. Spectra were acquired over a range of *m*/*z* 50−3000; several scans were averaged to provide the final spectrum.

Synthesis of L*56 (See Scheme 1). A solution of the chiral 2-acetylpyridine derivative **B**[13] (1.06 g, 4.95 mmol) in *N*,*N*′-dimethylformamide-dimethylacetal (3 cm^3) was heated to 120 °C overnight to give an orange oil; the addition of an equal volume of hexane and immersion in an ultrasound bath resulted in precipitation of the enone **C** as a cream solid, which was filtered off and dried (1.07 g, 80%). ESMS: *m*/*z* 270 (M^+). ^{1}H NMR ($CDCl_3$, 250 MHz): δ 7.88 (1H, d, J = 12.5 Hz, alkenyl H), 7.84 (1H, d, J = 7.6 Hz, pyridyl H^3), 7.29 (1H, d, J = 7.6 Hz, pyridyl H^4), 6.46 (1H, d, J = 12.8 Hz, alkenyl H), 3.25−2.93 (8H, m, $N(CH_3)_2$ and pyridyl^6−CH_2), 2.80 (1H, pseudo-t, J = 5.6 Hz, pyridyl^5−C*H*), 2.73−2.62 (1H, m, CH−CH_2−CH), 2.42−2.32 (1H, m, pyridyl^6−CH_2−C*H*), 1.40 (3H, s, pinene CH_3), 1.26 (1H, d, J = 9.8 Hz, CH−CH_2−CH), 0.63 (3H, s, pinene CH_3).

A solution of enone **C** (2.24 g, 8.30 mmol) and hydrazine monohydrate (2.8 cm^3, 58 mmol) in ethanol (4 cm^3) was heated to 60 °C for 30 min. The addition of water (20 cm^3) resulted in precipitation of a cream solid, which was extracted with several portions of CH_2Cl_2; the extracts were combined and dried to give the pyridyl−pyrazole **D** in 95% yield. ESMS: *m*/*z* 239 (M^+). ^{1}H NMR ($CDCl_3$, 250 MHz): δ 7.62 (1H, d, J = 2.1 Hz, pyrazolyl H^5), 7.37 (1H, d, J = 7.9 Hz, pyridyl H^3), 7.25 (1H, d, J = 7.6 Hz,

Table 1. Crystallographic Data for the Nine Structures

complex	$[Cu(L^{naph})](OTf)$	$[Ag(L^{naph})](BF_4)$	$[Cu_4(L^{naph})_4](BF_4)_4\cdot 2MeCN\cdot {}^{i}Pr_2O$
formula	$C_{29}H_{22}CuF_3N_6O_3S$	$C_{28}H_{22}AgBF_4N_6$	$C_{122}H_{108}B_4Cu_4F_{16}N_{26}O$
fw	655.13	637.19	2555.74
T (K)	150(2)	150(2)	150(2)
λ (Å)	0.710 73	0.710 73	0.710 73
cryst syst	orthorhombic, *Pbca*	monoclinic, $P2_1/n$	monoclinic, $P2_1/n$
a (Å)	17.757(2)	8.394(2)	20.181(4)
b (Å)	13.4265(16)	12.884(3)	29.464(5)
c (Å)	22.179(3)	23.554(6)	20.464(4)
α (deg)	90	90	90
β (deg)	90	94.353(4)	90.514(3)
γ (deg)	90	90	90
V (Å^3)	5287.7(11)	2540.1(10)	12168(4)
Z	8	4	4
D_{calcd} (Mg/m^3)	1.646	1.666	1.395
μ (mm^{-1})	0.973	0.854	0.775
cryst size (mm)	0.45 × 0.20 × 0.15	0.40 × 0.15 × 0.08	0.40 × 0.15 × 0.10
data/restraints/param	6072/0/388	5791/0/361	27 959/18/1599
R1, wR2	0.0492, 0.1349	0.0388, 0.0934	0.0699, 0.1908
largest diff peak and hole (e/Å^3)	0.449, −0.774	0.540, −0.386	0.759, −0.923

complex	$[Cu_{12}(L^{naph})_{18}](ClO_4)_{24}\cdot 7.5MeCN$[a]	$[Cd_{12}(L^{naph})_{18}](BF_4)_{24}\cdot 6Et_2O\cdot 4.5MeCN\cdot 4H_2O$	$[Cu(L^{*45})](BF_4)\cdot MeCN$
formula	$C_{519}H_{418.5}Cl_{16.50}Cu_{12}N_{115.5}O_{66}$	$C_{537}H_{477.5}B_{24}Cd_{12}F_{96}\ N_{112.5}O_{10}$	$C_{44}H_{45}BCuF_4N_7$
fw	10 676.60	12 099.06	822.22
T (K)	100(2)	100(2)	120(2)
λ (Å)	1.541 78	1.541 78	0.710 73
cryst syst	hexagonal, $P6_3$	hexagonal, $P6_3$	orthorhombic, $C222_1$
a (Å)	29.5522(18)	29.3977(7)	19.4078(10)
b (Å)	29.5522(18)	29.3977(7)	20.6529(9)
c (Å)	91.693(12)	92.802(4)	9.8969(5)
α (deg)	90	90	90
β (deg)	90	90	90
γ (deg)	120	120	90
V (Å^3)	69 350(11)	69 457(4)	3966.9(3)
Z	4	4	4
D_{calcd} (Mg/m^3)	1.023	1.157	1.377
μ (mm^{-1})	1.474	3.558	0.611
cryst size (mm)	0.20 × 0.15 × 0.10	0.35 × 0.3 × 0.1	0.18 × 0.16 × 0.06
data/restraints/param	34 904/12 062/2020	78 362/378/2241	4554/8/260
R1, wR2	0.1536, 0.3661	0.1124, 0.3335	0.0601, 0.1537
largest diff peak and hole (e/Å^3)	0.554, −0.822	1.398, −1.327	+0.581, −0.722

complex	$[Ag(L^{*45})](ClO_4)\cdot MeCN$	$[Ag_4(L^{*56})_4](BF_4)_4\cdot (H_2O)_{0.5}$	$[Zn_4(L^{*45})_6](ClO_4)_8$[a]
formula	$C_{44}H_{45}AgClN_7O_4$	$C_{168}H_{169}N_{24}Ag_4B_4F_{16}O_{0.5}$	$C_{252}H_{252}Cl_3N_{36}O_{12}Zn_4$
fw	879.19	3310.99	4344.73
T (K)	150(2)	100(2)	100(2)
λ (Å)	0.710 73	0.710 73	0.710 73
cryst syst	orthorhombic, $C222_1$	tetragonal, $P4$	cubic, $F4_132$
a (Å)	18.746(3)	24.3896(7)	38.238(5)
b (Å)	21.315(4)	24.3896(7)	38.238(5)
c (Å)	10.2088(17)	13.3039(9)	38.238(5)
α (deg)	90	90	90
β (deg)	90	90	90
γ (deg)	90	90	90
V (Å^3)	4079.1(12)	7913.9(6)	55909(13)
Z	4	2	8
D_{calcd} (Mg/m^3)	1.432	1.389	1.032
μ (mm^{-1})	0.612	0.566	0.424
cryst size (mm)	0.42 × 0.12 × 0.08	0.20 × 0.15 × 0.10	0.25 × 0.25 × 0.25
data/restraints/param	4640/5/271	13376/1312/942	1448/234/266
R1, wR2	0.0431, 0.0926	0.0897, 0.2819	0.1244, 0.3219
largest diff peak and hole (e/Å^3)	+0.0628, −0.824	+1.45, −1.21	+0.766, −0.823

[a] Not all of the anions could be located because of extensive disorder; the molecular formula, formula weight, and density are based on what could actually be located. A SQUEEZE function was applied (see the Experimental Section for further details).

pyridyl H^4), 6.69 (1H, d, J = 1.8 Hz, pyrazolyl H^4), 3.15−3.10 (2H, m, pyridyl^6−CH_2), 2.81−2.73 (1H, m, pyridyl^5−C*H*), 2.73−2.84 (1H, m, CH−CH_2−CH), 2.42−2.34 (1H, m, pyridyl^6−CH_2−C*H*), 1.41 (3H, s, CH_3), 1.27 (1H, d, J = 9.5 Hz, CH−CH_2−CH), 0.66 (3H, s, CH_3).

A mixture of 1,8-bis(bromomethyl)naphthalene (1.97 g, 6.28 mmol) and the pyridyl−pyrazole **D** (3.01 g, 12.6 mmol), aqueous NaOH (10 M, 15 cm^3), toluene (80 cm^3), and Bu_4NOH (40% aqueous solution, three drops) was stirred vigorously (overhead stirrer) at 60 °C for 30 min. The mixture was then further diluted

Table 2. Selected Bond Distances (Å) and Angles (deg) for $[Cu(L^{naph})](OTf)$

Cu(1)−N(61)	2.001(3)
Cu(1)−N(21)	2.017(3)
Cu(1)−N(11)	2.051(3)
Cu(1)−N(51)	2.074(3)
N(61)−Cu(1)−N(21)	141.07(12)
N(61)−Cu(1)−N(11)	117.25(12)
N(21)−Cu(1)−N(11)	80.92(12)
N(61)−Cu(1)−N(51)	80.37(11)
N(21)−Cu(1)−N(51)	104.39(11)
N(11)−Cu(1)−N(51)	145.22(12)

Table 3. Selected Bond Distances (Å) and Angles (deg) for $[Ag(L^{naph})](BF_4)$

Ag(1)−N(51)	2.147(2)
Ag(1)−N(11)	2.152(2)
Ag(1)···N(61)	2.707(2)
Ag(1)···N(21)	2.798(2)
N(51)−Ag(1)−N(11)	175.79(9)

with water (60 cm^3), and the organic layer was separated, dried over $MgSO_4$, and evaporated to dryness. The residue was purified by column chromatography on alumina using CH_2Cl_2−THF (95:5, v/v) as the eluent to give pure L*[56] in 74% yield. ESMS: *m*/*z* 630 (M^+). Anal. Calcd for $C_{42}H_{42}N_6(H_2O)_{0.5}$: C, 78.8; H, 6.8; N, 13.1. Found: C, 78.8; H, 6.7; N, 12.8. ^{1}H NMR (250 MHz, $CDCl_3$): δ 7.89 (2H, dd, J = 8.2 and 1.2 Hz, naphthyl H^2 and H^7 or H^4 and H^5), 7.67 (2H, d, J = 7.9 Hz, pyridyl H^3), 7.43 (2H, dd, J = 8.2 and 7.0 Hz, naphthyl H^3 and H^6), 7.26 (2H, d, J = 7.6 Hz, pyridyl H^4), 7.20 (2H, d, J = 7.0 Hz, naphthyl H^4 and H^5 or H^2 and H^7), 7.13 (2H, d, J = 2.1 Hz, pyrazolyl H^5), 6.93 (2H, br s, pyrazolyl H^4), 5.92 (4H, s, CH_2), 3.25−3.16 (4H, m, pyridyl^6−C*H*$_2$), 2.81−2.74 (2H, m, pyridyl^5−C*H*), 2.73−2.62 (2H, m, CH−C*H*$_2$−CH), 2.42−2.32 (2H, m, pyridyl^6−CH_2−C*H*), 1.39 (6H, s, CH_3), 1.28 (2H, d, J = 9.5 Hz, CH−C*H*$_2$−CH), 0.66 (6H, s, CH_3).

Synthesis of L*[45] (See Scheme 1). This was prepared in exactly the same way as that described above for the final step of the synthesis of L*[56], using 1,8-bis(bromomethyl)naphthalene and 2 equiv of **A** to give L*[45] in 68% yield. ESMS: *m*/*z* 630 (M^+). Calcd for $C_{42}H_{42}N_6\cdot1.5H_2O$: C, 76.7; H, 6.9; N, 12.8. Found: C, 76.5; H, 6.8; N, 12.3. ^{1}H NMR (270 MHz, $CDCl_3$): δ 8.15 (2H, s, pyridyl H^6), 7.91 (2H, dd, J = 8.2 and 1.2 Hz, naphthyl H^2 and H^7 or H^4 and H^5), 7.80 (2H, s, pyridyl H^3), 7.45 (2H, td, J = 8.2 and 1.2 Hz, naphthyl H^3 or H^6), 7.21 (2H, dd, J = 7.3 and 1.2 Hz, naphthyl H^4 and H^5 or H^2 and H^7), 7.14 (2H, d, J = 2.1 Hz, pyrazolyl H^5), 6.87 (2H, d, J = 2.1 Hz, pyrazolyl H^4), 5.93 (4H, s, CH_2), 3.02−2.97 (4H, m, pyridyl^4−C*H*$_2$), 2.83 (2H, t, J = 5.3 Hz, CH−C*H*$_2$−CH), 2.69 (2H, dt, J = 9.5 and 5.5 Hz, CH−C*H*$_2$−CH), 2.33−2.24 (2H, m, pyridyl^4−CH_2−C*H*), 1.40 (6H, s, CH_3), 1.22 (2H, d, J = 9.8 Hz, pyridyl^5−C*H*), 0.64 (6H, s, CH_3).

Syntheses of Complexes. Complexes were prepared by the reaction of the ligand with the appropriate metal salt [in a 1:1 metal−ligand ratio for the Cu^I and Ag^I complexes and in a 2:3 ratio for the Cu^{II}, Zn^{II}, and Cd^{II} complexes] in dry MeCN. Diffusion of diethyl ether or diisopropyl ether vapor into the resulting solutions afforded a crystalline product in every case. ESMS spectra of the complexes are discussed in the main text. Elemental analytical data on vacuum-dried samples are as follows. Note that, for the two cage complexes, the observed % C figure is about 1% low; however, if we assume absorption of 10 molecules of water in each case, thenthe analyses fall within acceptable limits.

$[Cu(L^{naph})](OTf)$. Anal. Calcd for $C_{29}H_{22}CuF_3N_6O_3S$: C, 53.2; H, 3.4; N, 12.8. Found: C, 52.4; H, 3.3; N, 12.7.

Table 4. Selected Bond Distances (Å) and Angles (deg) for $[Cu_4(L^{naph})_4](BF_4)_4\cdot2MeCN\cdot{}^iPr_2O$

Cu(1)−N(111)	2.007(4)	N(111)−Cu(1)−N(461)	142.34(19)
Cu(1)−N(461)	2.015(5)	N(111)−Cu(1)−N(451)	125.48(17)
Cu(1)−N(451)	2.028(4)	N(461)−Cu(1)−N(451)	80.8(2)
Cu(1)−N(121)	2.066(4)	N(111)−Cu(1)−N(121)	80.10(18)
		N(461)−Cu(1)−N(121)	120.24(18)
		N(451)−Cu(1)−N(121)	108.27(16)
Cu(2)−N(211)	2.012(4)	N(211)−Cu(2)−N(151)	127.45(17)
Cu(2)−N(151)	2.014(4)	N(211)−Cu(2)−N(161)	136.24(18)
Cu(2)−N(161)	2.016(5)	N(151)−Cu(2)−N(161)	80.90(18)
Cu(2)−N(221)	2.041(4)	N(211)−Cu(2)−N(221)	80.17(18)
		N(151)−Cu(2)−N(221)	113.17(16)
		N(161)−Cu(2)−N(221)	122.55(17)
Cu(3)−N(251)	1.980(4)	N(251)−Cu(3)−N(311)	135.31(17)
Cu(3)−N(311)	2.001(4)	N(251)−Cu(3)−N(321)	116.06(16)
Cu(3)−N(321)	2.049(4)	N(311)−Cu(3)−N(321)	80.77(17)
Cu(3)−N(261)	2.058(4)	N(251)−Cu(3)−N(261)	80.86(17)
		N(311)−Cu(3)−N(261)	130.26(17)
		N(321)−Cu(3)−N(261)	117.22(16)
Cu(4)−N(351)	2.012(4)	N(351)−Cu(4)−N(411)	130.24(17)
Cu(4)−N(411)	2.024(4)	N(351)−Cu(4)−N(421)	118.22(17)
Cu(4)−N(421)	2.026(4)	N(411)−Cu(4)−N(421)	80.02(17)
Cu(4)−N(361)	2.030(4)	N(351)−Cu(4)−N(361)	80.24(17)
		N(411)−Cu(4)−N(361)	132.82(17)
		N(421)−Cu(4)−N(361)	120.43(17)

Table 5. Selected Bond Distances (Å) for $[Cu_{12}(L^{naph})_{18}](ClO_4)_{24}\cdot7.5MeCN$

Cu(1)−N(11A)	2.002(9)	Cu(5)−N(11G)	1.962(10)
Cu(1)−N(11E)	2.060(9)	Cu(5)−N(11K)	2.048(10)
Cu(1)−N(21A)	2.060(8)	Cu(5)−N(21G)	2.212(10)
Cu(1)−N(61C)	2.070(10)	Cu(5)−N(51I)	2.212(11)
Cu(1)−N(21E)	2.286(9)	Cu(5)−N(21K)	2.218(12)
Cu(1)−N(51C)	2.381(9)	Cu(5)−N(61I)	2.236(12)
Cu(2)−N(11B)	1.989(10)	Cu(6)−N(11H)	2.007(9)
Cu(2)−N(61D)	2.030(10)	Cu(6)−N(61J)	2.011(9)
Cu(2)−N(21B)	2.170(9)	Cu(6)−N(51J)	2.216(11)
Cu(2)−N(51D)	2.227(9)	Cu(6)−N(51G)	2.222(10)
Cu(2)−N(61A)	2.250(18)	Cu(6)−N(21H)	2.229(10)
Cu(2)−N(51A)	2.259(15)	Cu(6)−N(61G)	2.294(11)
Cu(3)−N(11D)	1.985(10)	Cu(7)−N(11J)	2.021(9)
Cu(3)−N(11C)	2.010(9)	Cu(7)−N(11I)	2.045(9)
Cu(3)−N(21C)	2.182(9)	Cu(7)−N(21I)	2.047(9)
Cu(3)−N(21D)	2.204(10)	Cu(7)−N(61H)	2.079(9)
Cu(3)−N(61B)	2.215(12)	Cu(7)−N(21J)	2.299(9)
Cu(3)−N(51B)	2.292(11)	Cu(7)−N(51H)	2.379(9)
Cu(4)−N(61E)	2.024(9)	Cu(8)−N(61K)	2.020(9)
Cu(4)−N(61F)	2.029(10)	Cu(8)−N(11L)	2.042(9)
Cu(4)−N(51F)	2.161(9)	Cu(8)−N(21L)	2.103(9)
Cu(4)−N(11F)	2.212(9)	Cu(8)−N(61L)	2.111(9)
Cu(4)−N(51E)	2.215(10)	Cu(8)−N(51K)	2.278(9)
Cu(4)−N(21F)	2.298(9)	Cu(8)−N(51L)	2.371(9)

$[Ag(L^{naph})](BF_4)$. Anal. Calcd for $C_{28}H_{22}AgBF_4N_6$: C, 52.8; H, 3.5; N, 13.2. Found: C, 52.8; H, 3.3; N, 13.2.

$[Cu_4(L^{naph})_4](BF_4)_4\cdot2.5H_2O$. Anal. Calcd for $C_{112}H_{88}B_4Cu_4F_{16}N_{24}\cdot2.5H_2O$: C, 55.6; H, 3.9; N, 13.9. Found: C, 55.1; H, 3.7; N, 13.7.

$[Cu_{12}(L^{naph})_{18}](ClO_4)_{24}$. Anal. Calcd for $C_{504}H_{396}Cl_{24}Cu_{12}N_{108}O_{96}$: C, 54.5; H, 3.6; N, 13.6. Found: C, 53.6; H, 3.9; N, 13.5.

$[Cd_{12}(L^{naph})_{18}](BF_4)_{24}$. Anal. Calcd for $C_{504}H_{396}B_{24}Cd_{12}F_{96}N_{108}$: C, 53.1; H, 3.5; N, 13.3. Found: C, 52.0; H, 3.6; N, 12.9.

$[Cu(L^{*45})](BF_4)$. Anal. Calcd for $C_{42}H_{42}N_6CuBF_4$: C, 64.6; H, 5.4; N, 10.8. Found: C, 64.2; H, 5.2; N, 10.8.

$[Ag(L^{*45})](ClO_4)$. Anal. Calcd for $C_{42}H_{42}N_6AgClO_4$: C, 60.2; H, 5.1; N, 10.0. Found: C, 59.7; H, 5.0; N, 9.8.

$[Ag_4(L^{*56})_4](BF_4)_4\cdot8H_2O$. Anal. Calcd for $C_{168}H_{184}N_{24}O_8Ag_4B_4F_{16}$: C, 58.5; H, 5.4; N, 9.8. Found: C, 57.8; H, 5.4; N, 9.8.

$[Zn_4(L^{*45})_6](ClO_4)_8$. Anal. Calcd for $C_{252}H_{252}N_{36}Cl_8O_{32}Zn_4$: C, 62.5; H, 5.2; N, 10.4. Found: C, 62.0; H, 5.0; N, 10.0.

X-ray Crystallography. The data for the structure of $[Cu(L^{*45})](BF_4)\cdot$MeCN were collected by Dr. Peter Horton at the National

Table 6. Selected Bond Distances (Å) for $[Cd_{12}(L^{naph})_{18}](BF_4)_{24}\cdot 6Et_2O\cdot 4.5MeCN\cdot 4H_2O$

Cd(1)−N(51C)	2.280(12)	Cd(5)−N(11G)	2.297(13)
Cd(1)−N(21A)	2.317(12)	Cd(5)−N(41I)	2.299(13)
Cd(1)−N(21D)	2.333(11)	Cd(5)−N(21J)	2.323(11)
Cd(1)−N(41C)	2.341(11)	Cd(5)−N(21G)	2.340(10)
Cd(1)−N(11D)	2.386(12)	Cd(5)−N(11J)	2.349(11)
Cd(1)−N(11A)	2.390(12)	Cd(5)−N(51I)	2.361(13)
Cd(2)−N(51B)	2.298(11)	Cd(6)−N(11H)	2.276(11)
Cd(2)−N(41F)	2.323(13)	Cd(6)−N(41L)	2.302(10)
Cd(2)−N(21C)	2.332(12)	Cd(6)−N(41G)	2.325(11)
Cd(2)−N(51F)	2.343(14)	Cd(6)−N(51L)	2.331(10)
Cd(2)−N(41B)	2.343(11)	Cd(6)−N(51G)	2.366(11)
Cd(2)−N(11C)	2.384(13)	Cd(6)−N(21H)	2.370(10)
Cd(3)−N(51A)	2.281(10)	Cd(7)−N(11L)	2.299(13)
Cd(3)−N(21F)	2.304(10)	Cd(7)−N(11I)	2.300(12)
Cd(3)−N(11B)	2.330(12)	Cd(7)−N(21L)	2.319(11)
Cd(3)−N(41A)	2.340(10)	Cd(7)−N(41H)	2.327(13)
Cd(3)−N(11F)	2.347(10)	Cd(7)−N(21I)	2.344(10)
Cd(3)−N(21B)	2.353(10)	Cd(7)−N(51H)	2.357(13)
Cd(4)−N(11E)	2.267(10)	Cd(8)−N(51K)	2.301(11)
Cd(4)−N(51D)	2.325(11)	Cd(8)−N(41J)	2.306(12)
Cd(4)−N(41D)	2.329(11)	Cd(8)−N(51J)	2.323(11)
Cd(4)−N(41E)	2.336(10)	Cd(8)−N(21K)	2.351(10)
Cd(4)−N(21E)	2.362(10)	Cd(8)−N(11K)	2.366(10)
Cd(4)−N(51E)	2.387(11)	Cd(8)−N(41K)	2.371(10)

Table 7. Selected Bond Distances (Å) and Angles (deg) for $[Cu(L^{*45})](BF_4)\cdot MeCN$

Cu(1)−N(11)	2.035(3)
Cu(1)−N(21)	2.079(3)
N(11)−Cu(1)−N(11A)	116.20(19)
N(11)−Cu(1)−N(21)	80.60(13)
N(11)−Cu(1)−N(21A)	145.70(14)
N(21)−Cu(1)−N(21A)	102.33(18)

Table 8. Selected Bond Distances (Å) and Angles (deg) for $[Ag(L^{*45})](ClO_4)\cdot MeCN$

Ag(1)−N(21)	2.233(3)
Ag(1)−N(31)	2.495(3)
N(21)−Ag(1)−N(21A)	150.17(16)
N(21)−Ag(1)−N(31)	72.03(10)
N(21)−Ag(1)−N(31A)	133.51(11)
N(31)−Ag(1)−N(31A)	84.87(13)

Crystallography Service, University of Southampton, on a Nonius-Kappa CCD diffractometer using Mo Kα radiation from a Bruker-Nonius FR591 rotating-anode X-ray generator. The data were absorption-corrected using SORTAV,[20] before solution and refinement using *SHELXS-97* and *SHELXL-97*, respectively.[21,22] All other crystals were quickly coated in oil and transferred to a diffractometer (either a Bruker-AXS SMART 1000 with Mo Kα radiation, a Bruker-AXS SMART 4000 with Mo Kα radiation, or a Bruker-AXS PROTEUM, with a rotating-anode source producing Cu Kα radiation), where they were mounted under a stream of cold N_2. Crystals of the cage complexes in particular were heavily solvated and started to decompose instantly upon removal from the mother liquor so the transfer was effected as quickly as possible. After integration of the raw data and merging of equivalent reflections, an empirical absorption correction was applied using *SADABS*.[23] The structures were solved by direct methods and refined by full-matrix least squares on weighted F^2 values for all reflections using the *SHELX* suite of programs.[21,22] Details of the crystal properties, data collection, and refinements are collected in Table 1.

Table 9. Selected Bond Distances (Å) and Angles (deg) for $[Ag_4(L^{*56})_4](BF_4)_4\cdot(H_2O)_{0.5}$

Ag(1)−N(61A)	2.306(6)	Ag(2)−N(61B)	2.317(10)
Ag(1)−N(11A)	2.308(7)	Ag(2)−N(11B)	2.317(9)
Ag(1)−N(21A)	2.325(7)	Ag(2)−N(51B)	2.382(11)
Ag(1)−N(51A)	2.353(7)	Ag(2)−N(21B)	2.412(11)
N(61A)−Ag(1)−N(11A)	144.6(3)	N(61B)−Ag(2)−N(11B)	147.3(3)
N(61A)−Ag(1)−N(21A)	135.5(3)	N(61B)−Ag(2)−N(51B)	71.0(4)
N(11A)−Ag(1)−N(21A)	71.6(3)	N(11B)−Ag(2)−N(51B)	135.6(3)
N(61A)−Ag(1)−N(51A)	71.4(2)	N(61B)−Ag(2)−N(21B)	130.0(3)
N(11A)−Ag(1)−N(51A)	127.8(3)	N(11B)−Ag(2)−N(21B)	72.4(3)
N(21A)−Ag(1)−N(51A)	109.3(2)	N(51B)−Ag(2)−N(21B)	98.6(4)

Table 10. Selected Bond Distances (Å) and Angles (deg) for $[Zn_4(L^{*45})_6](ClO_4)_8$

Zn(1)−N(11)	2.100(12)
Zn(1)−N(21)	2.221(11)
N(11)−Zn(1)−N(11A)	96.4(4)
N(11)−Zn(1)−N(21B)	90.3(4)
N(11)−Zn(1)−N(21)	78.3(5)
N(11)−Zn(1)−N(21A)	171.9(5)
N(21)−Zn(1)−N(21A)	95.5(3)

For $[Cu_{12}(L^{naph})_{18}](ClO_4)_{24}\cdot 7.5MeCN$, the diffraction data were particularly weak because of a combination of solvent loss from the crystal and extensive disorder of the anions; only 16.5 of the required 24 perchlorate anions could be clearly located (the crystal formula and formula mass in Table 1 reflect this). The SQUEEZE function in PLATON was used to account for regions of diffuse electron density that could not be satisfactorily modeled. For both dodecanuclear cage complexes (Cu and Cd), geometric similarity restraints (SAME) were applied to all pyrazolyl−pyridine, phenyl-ring, tetrahedral anions, and solvent moieties to assist in the refinement. H atoms for these two structures were included in calculated positions for the ligands but not for lattice solvent molecules. Only the metal atoms (Cu or Cd) could be refined with anisotropic thermal parameters; all other atoms were refined isotropically.

Similar problems occurred with $[Zn_4(L^{*45})_6](ClO_4)_8$; although it formed well-shaped substantial crystals, they lost solvent rapidly and scattered very weakly. Only three out of the eight expected perchlorate anions could be located (of which one is in the central cavity); the rest were badly disordered and no doubt mixed up with disordered solvent molecules. The SQUEEZE function in PLATON was again used to eliminate regions of diffuse electron density that could not be satisfactorily modeled. The structure of the cationic complex cage is however clear.

Selected bond distances and angles are given in Tables 2−10.

Acknowledgment. We thank EPSRC and University of Sheffield for financial support and Dr. Peter Horton and Prof. Mike Hursthouse of the EPSRC National Crystallography Service, University of Southampton, for the data collection on $[Cu(L^{*45})](BF_4)\cdot MeCN$.

Supporting Information Available: Crystallographic data in CIF format. This material is available free of charge via the Internet at http://pubs.acs.org.

IC060157D

(20) Blessing, R. H. *Acta Crystallogr.* **1995**, *A51*, 33. Blessing, R. H. *J. Appl. Crystallogr.* **1997**, *30*, 421.
(21) Sheldrick, G. M. *SADABS*: *A program for absorption correction with the Siemens SMART system*; University of Göttingen: Göttingen, Germany, 1996.
(22) *SHELXTL program system*, version 5.1; Bruker Analytical X-ray Instruments Inc.: Madison, WI, 1998.
(23) Sheldrick, G. M. *SADABS, A program for absorption correction with the Siemens SMART area-detector system*; University of Göttingen: Göttingen: Germany, 1996.